Tectonic interpretation of transient stage erosion rates at different spatial scales in an uplifting block

S. Carretier,[1,2] B. Poisson,[3] R. Vassallo,[1,2,4] E. Pepin,[1] and M. Farias[5]

[1]   We explore the extent to which it is possible to convert erosion rate data into uplift rate or erosion laws, using a landscape evolution model. Transient stages of topography and erosion rates of a block uplifting at a constant rate are investigated at different spatial scales, for a constant climate, and for various erosion laws and initial topographies. We identify three main model types for the evolution of the mountain-scale mean erosion rate: "linear"-type, "sigmoid"-type and "exponential"-type. Linear-type models are obtained for topographies without drainage system reorganization, in which river incision rates never exceed the uplift rate and stepped river terraces converge upstream. In sigmoid-type and exponential-type models (typically detachment-limited or transport-limited models with a significant transport threshold), drainage growth lasts a long time, and correspond to more than linear transport laws in water discharge and slope. In exponential-type models, the mean erosion rate passes through a maximum that is higher than the rock uplift rate. This happens when the time taken to connect the drainage network exceeds half the total response time to reach dynamic equilibrium. River incision rates can be much greater than the uplift rate in both cases. In the exponential-type model, river terraces converge downstream. Observations of a mountain in the Gobi-Altay range in Mongolia support the exponential-type model. This suggests that the erosion of this mountain is either detachment-limited or transport-limited with a significant transport threshold. This study shows that drainage growth could explain differences in erosion rate measurements on different spatial scales in a catchment.

1.   Introduction

[2]   Many studies have attempted to convert erosion rates (ϵ [LT^{-1}]) into rock uplift rate (U [LT^{-1}]) [e.g., *Pazzaglia et al.*, 1998; *Hurtrez et al.*, 1999; *Lavé and Avouac*, 2000, 2001; *Pazzaglia and Brandon*, 2001; *Vassallo et al.*, 2007b]. This is a difficult task for two reasons: first of all, the timescale for which the mean erosion rates are representative of tectonic processes is not well known. Comparisons between erosion rates for different timescales have resulted in significant differences due to the under-sampling of major erosion events or to climate-driven variations [*Kirchner et al.*, 2001; *von Blanckenburg*, 2005]. Second, the erosion rate equals the rock uplift rate only if a dynamic equilibrium has been reached, which may not be true in many active mountains with significant climatic variations or if response times are especially long

[*Whittaker et al.*, 2007a; *Stolar et al.*, 2007b; *Farías et al.*, 2008; *Cowie et al.*, 2008]. For these two reasons, the erosion rate can be greater or smaller than the rock uplift rate. It can be greater if climate change has led to increasing river incision [*Zaprowski et al.*, 2005] or because of a sudden base level fall at the mountain piedmont [*Carretier and Lucazeau*, 2005; *Vassallo et al.*, 2007b]. It can be smaller in the case of a catchment with slopes that have not yet reached their equilibrium [*Kooi and Beaumont*, 1996]. The interpretation of erosion rates is also a spatial-scale problem. During the phase of adjustment to uplift, erosion evolves at different rates along the catchment, so that parts of the system may have reached a dynamic equilibrium ($\epsilon = U$) while other parts of the system have not [*Whipple and Tucker*, 1999]. Consequently, the local incision rate, as deduced from river terraces, may differ significantly from the mean catchment-scale erosion rate over the same time period, without any necessary variations in rock uplift rates within the catchment. Recent advances in thermochronology and cosmogenic nuclide-derived erosion rates and terrace dating represent an opportunity to compare erosion rates for different temporal and spatial scales. Physical and numerical modeling of erosion in active mountain belts shed light on the coupling relationship between relief, erosion rate, tectonics and climate, particularly during the dynamic equilibrium stage [*Howard et al.*, 1994; *Densmore et al.*,

[1]LMTG, UPS (OMP), Université de Toulouse, Toulouse, France.
[2]Also at IRD, Toulouse, France.
[3]Hazard Mechanisms and Simulation Unit, Bureau de Recherches Géologiques et Minières, Orleans, France.
[4]Now at LGCA, Université de Savoie, le Bourget du Lac, France.
[5]Departamento de Geología, Universidad de Chile, Santiago, Chile.

1998; *Willett*, 1999; *Whipple and Tucker*, 1999; *Davy and Crave*, 2000; *Tucker*, 2004; *Stolar et al.*, 2007a]. However, only a few studies have examined the evolution of erosion rates on different spatial scales or within embedded systems (catchment, hillslope, river network) during transient response to uplift [e.g., *Anderson*, 1994; *Kooi and Beaumont*, 1996; *Lague*, 2001; *Whipple and Tucker*, 2002; *van der Beek et al.*, 2002; *Carretier and Lucazeau*, 2005; *Tucker and Whipple*, 2002; *Gasparini et al.*, 2006]. Thus, a theoretical framework that links erosion rate data on different spatial scales within a catchment is still missing.

[3] In this paper, we address the following question: what controls the shape of an ϵ versus time curve? We explore the hypothesis that (1) erosion rates on a steadily rising block may following one of a small number of characteristic patterns, and (2) these patterns involve systematic changes over time in the relationship between erosion rate and rock uplift rate. Analyzing these changes, we evaluate if it is possible to extract information about uplift rate and erosion laws from topographic and erosion rate data on different spatial scales from a catchment in a transient state. We investigate the relationships between the mountain-scale erosion rate, local-scale river incision rate, and river transient profiles in the case of an uplifting surface with a constant area and subject to constant and homogeneous uplift and climate. Restricting the study to a constant climate is for the sake of simplicity. Thus, erosion rates are calculated over timescales that express average global climate variations.

[4] We use a landscape evolution model (CIDRE), which allows diffusive and advection transport to be modeled over geological time spans. We analyze the effect of erosion laws and the initial topography on the evolution of topography and erosion rates.

2. Model

[5] The CIDRE model is a modified C++ version of the model used by [*Carretier and Lucazeau*, 2005]. It belongs to the family of cellular automaton models [e.g. *Willgoose et al.*, 1991a; *Kooi and Beaumont*, 1994; *Howard et al.*, 1994; *Tucker and Bras*, 2000; *Nicholas and Quine*, 2007] with local rules of square cell interactions governing the overall evolution of the system. Notations are summarized in Table 1.

[6] Hydrology is modeled by propagating a specified volume of water per unit of time downstream from the highest to the lowest cell, in order to ensure water conservation in the drainage network. For each cell, the water flux Q $[L^3T^{-1}]$ is the sum of all incoming water fluxes from upstream draining cells, as well as the local precipitation:

$$Q = \sum_i P_i \Delta x^2 + P \Delta x^2 \qquad (1)$$

where Δx $[L]$ is the cell width, P_i and P $[LT^{-1}]$ are the rates of precipitation over the upstream cells i, and the local precipitation rate, respectively. In holes, water disappears entirely for the purpose of the present study. Neglecting water accumulation in lakes can have potential impact on our results, which we discuss in section 5.2.

[7] In order to take water dispersion on gently dipping surfaces into account, a multiple flow algorithm is used: the water outflux Q_j $[L^3T^{-1}]$ toward each lower neighboring cell j is calculated by [e.g., *Murray and Paola*, 1997; *Pelletier*, 2004; *Carretier and Lucazeau*, 2005]

$$Q_j = Q \frac{S_j}{\sum_j S_j} \qquad (2)$$

in which S_j is the slope toward a cell j. The number of cells j depends on the topography. It is usually 3 or 4 on hillslopes and is generally reduced to one in a river network, as with the "steepest-descent" algorithm.

[8] Processes involving small transport distances, such as soil creep and small landslides, are modeled using a transport rate per unit width qd_j $[L^2T^{-1}]$ toward each lower neighboring cell j, which is assumed to depend nonlinearly on the local elevation gradient [*Roering et al.*, 1999]:

$$qd_j = -\kappa \frac{S_j}{1 - (S_j/S_c)^2} \qquad (3)$$

where κ $[L^2T^{-1}]$ is a diffusion coefficient, S_c is the critical slope corresponding to the material gradient of repose. In the case of bedrock, the use of this law assumes that the weathering rate is sufficient to erode the bedrock at the rate determined by κ, and that bedrock collapses for slopes approaching S_c. A linear approximation of this law is used for slopes greater than $0.95S_c$ to prevent infinite flux.

[9] Sediment and bedrock layers have distinct lithological characteristics. The transport rate of sediments carried by water is determined by the specific transport capacity expressed as a sediment flux per unit width qt_j $[L^2T^{-1}]$

$$qt_j = K_{all} \left[k_t \left(\frac{Q_j}{W_j} \right)^m S_j^n - \tau_c \right]^p \qquad (4)$$

where W_j is the flow width $[L]$ in each lower direction j, and τ_c is a transport threshold, while other parameters are positive constants. The flow width W_j $[L]$ in each lower direction j is assumed to scale with the corresponding water flux volume:

$$W_j = k_w Q_j^{0.5} \qquad (5)$$

where k_w is a constant.

[10] Equation (4) can be viewed as a development of the classic form of the excess shear stress formula $(qt_j = K_{all}(\tau - \tau_c)^p)$, assuming uniform flow conditions, Manning or Chezy friction laws and a small depth to width hydraulic geometry [*Tucker*, 2004]. In this case, τ_c $[ML^{-1}T^{-2}]$ is a critical shear stress for clast entrainment, k_t, m and n are linked to the Manning or Chezy friction parameters, and K_{all} is an alluvial transport coefficient (see, e.g., *Tucker* [2004] for details).

[11] Bedrock detachment capacity I_j $[LT^{-1}]$ in direction j is expressed as [*Seidl and Dietrich*, 1992; *Howard*, 1997; *Whipple and Tucker*, 1999; *Tucker et al.*, 2001]

$$I_j = K_{br} \left[k_t \left(\frac{Q_j}{W_j} \right)^\alpha S_j^\beta - \tau_c \right]^a \qquad (6)$$

Table 1. Details of Model Parameters

Parameter	Dimension	Details of Parameters
A	$[L^2]$	drainage area
a	$[1]$	excess shear stress exponent (bedrock detachment law)
α	$[1]$	water discharge per unit width exponent (bedrock detachment law)
β	$[1]$	slope exponent (bedrock detachment law)
Δx	$[L]$	cell width (250 m)
Δz	$[L]$	elevation variation increment
Δt	$[T]$	time step (0.2–1 year)
ϵ	$[LT^{-1}]$	spatially averaged erosion rate
I_j	$[LT^{-1}]$	bedrock detachment rate capacity
k_t	$[ML^{-1-3m}T^{-2+m}]$	shear stress parameter (1400 Pa m$^{0.4}$ s$^{-1.3}$)
K_{br}	$[M^{-a}L^{1-a}T^{-1+2a}]$	bedrock detachment parameter
K_{sa}	$[L^{-1}]$	bedrock detachment parameter in the *Sklar and Dietrich*'s [2004] law
K_{all}	$[M^{-p}L^{2-p}T^{-1+2p}]$	transport capacity parameter
κ	$[L^2T^{-1}]$	diffusivity (10^{-2} m^2 a^{-1})
m	$[1]$	water discharge per unit width exponent (transport capacity law)
n	$[1]$	slope exponent (transport capacity law)
N_d, N_t	$[1]$	capacity-competence nondimensional numbers
N_{dt}	$[1]$	detachment versus transport-limited nondimensional number
NX, NY	$[1]$	number of row and lines, respectively.
p	$[1]$	excess shear stress exponent (transport capacity law)
P	$[LT^{-1}]$	precipitation rate (1 m a^{-1})
Q_j	$[L^3T^{-1}]$	volume water discharge toward cell j
Qs_{in}	$[L^3T^{-1}]$	sediment influx entering a cell
Qs	$[L^3T^{-1}]$	sediment influx leaving a cell
Qt	$[L^3T^{-1}]$	sum of the transport capacities in all directions
qs_j	$[L^2T^{-1}]$	sediment outflux per unit width toward j
qd_j	$[L^2T^{-1}]$	diffusion sediment capacity per unit width toward cell j
qt_j	$[L^2T^{-1}]$	transport capacity per unit width toward cell j
ρ_w	$[ML^{-3}]$	density of water
S	$[1]$	slope
S_c	$[1]$	critical slope for material collapse (0.6 for sediment and 1.7 for bedrock)
τ	$[ML^{-1}T^{-2}]$	shear stress
τ_c	$[ML^{-1}T^{-2}]$	critical shear stress
T_{co}	$[T]$	connectivity time
T	$[T]$	response time
U	$[LT^{-1}]$	uplift rate (1 mm a^{-1})
W_j	$[L]$	flow width in the direction toward cell j
w_f	$[LT^{-1}]$	water fall velocity of clast in still water
z	$[L]$	elevation

with α, β and a as positive constants and K_{br} representing a bedrock detachment coefficient. The detachment capacity can be viewed as deriving from the excess shear stress formula ($I_j = K_{br} (\tau - \tau_c)^a$), in which case $\alpha = m$ and $\beta = n$. The same critical shear stress τ_c is used for both bedrock detachment and sediment entrainment, although they can be set differently in the model.

[12] It is important to note that the dimension of K_{all} and K_{br} depends on p and a, which changes the meaning of these constants from one experiment to another and thus makes comparison difficult. It is easier to compare if the transport capacity and bedrock incision rates are nondimensionalized, as in Appendix A.

[13] In order to represent the fact that carried sediment can enhance ("tool effect") or inhibit ("cover effect") bedrock erosion, the following incision law can be used:

$$I_j = K_{sa}qs_j\left(1 - \frac{Q_s}{Qt}\right)\left[\frac{k_t\left(\frac{Q_j}{W_j}\right)^\alpha S_j^\beta}{\tau_c} - 1\right]^a\left[1 - \frac{k_t/\rho_w\left(\frac{Q_j}{W_j}\right)^\alpha S_j^\beta}{w_f}\right]^b \quad (7)$$

This is a development of the *Sklar and Dietrich*'s [2004] saltation-abrasion model, using the same assumptions as in equation (4). Q_s $[L^3T^{-1}]$ is the total sediment flux leaving the cell and Q_t $[L^3T^{-1}]$ is the sum of the transport capacities

in all lower directions. The flux q_{sj} $[L^2T^{-1}]$ is the sediment flux leaving the cell in direction j, w_f $[LT^{-1}]$ is the fall velocity of clasts in still water, K_{sa} is a bedrock detachment coefficient, ρ_w is the density of water and a and b are exponents. The incision rate I_j is the maximum for a shear stress value that falls between the critical shear stress for clast entrainment and a value for the passage from saltation (efficient for abrasion by impacts) to wash transport.

[14] Changes in elevation Δz are approximated by a finite volume approach [*Tucker et al.*, 2001]

$$\frac{\Delta z}{\Delta t} = U + \frac{1}{\Delta x^2}\left(Qs_{in} - \sum_j W_j qs_j\right) \quad (8)$$

where U $[LT^{-1}]$ is the rock uplift rate, Qs_{in} $[L^3T^{-1}]$ is the total sediment volume flux entering the cell, and the sum applies to all lower neighboring cells j. Also, Δt is the time increment, and the flow width W_j is determined by equation (5) in the case of water-driven transport or by the length of the side of the inset octagon within a cell ($(\sqrt{2} - 1)\Delta x$) in the case of small transport distance processes (equation (3)). Sediment outflux per unit width qs_j toward a lower cell j could be the result of sediment or bedrock erosion, or both. We describe this process on one cell in the following.

[15] The transport and detachment rates provided by equations (3), (4), and (6) or (7) are considered to be

Table 2. Tested Model Parameters[a]

Exp	NY	Initial Slope	K_{all} (10^{-5})	m	n	p	K_{br} (10^{-9})	α	β	a	τ_c	T_{co}	T	Type
						Threshold								
1	60	0	1.5	0.6	0.7	1.5	1.	0.6	0.7	1.5	1	0.035	0.08	SL
2	60	0	1.5	0.6	0.7	1.5	1.	0.6	0.7	1.5	5	0.17	0.28	E
3	60	0	1.5	0.6	0.7	1.5	1.	0.6	0.7	1.5	15	0.6	1.	E
4	60	0	1.5	0.6	0.7	1.5	1.	0.6	0.7	1.5	30	1.55	2.1	E
5	60	0	1.5	0.6	0.7	1.5	∞	-	-	-	0	0.015	2.	L
6	60	0	1.5	0.6	0.7	1.5	∞	-	-	-	2	0.055	0.11	E
7	60	0	1.5	0.6	0.7	1.5	∞	-	-	-	5	0.13	0.2	E
						Size System								
8	40	0	1.5	0.6	0.7	1.5	1.	0.6	0.7	1.5	30	1.2	1.6	E
9	50	0	1.5	0.6	0.7	1.5	1.	0.6	0.7	1.5	30	1.4	2	E
4	60	0	1.5	0.6	0.7	1.5	1.	0.6	0.7	1.5	30	1.55	2.1	E
10	60	0	60	2.	2.	1.	∞	-	-	-	0	2.		S
11	120	0	60	2.	2.	1.	∞	-	-	-	0	3.5	3.5	E
12	150	0	60	2.	2.	1.	∞	-	-	-	0	4.2	4.8	E
						Transport and Incision Coefficient								
4	60	0	1.5	0.6	0.7	1.5	1.	0.6	0.7	1.5	30	1.55	2.1	E
13	60	0	1.5	0.6	0.7	1.5	5.	0.6	0.7	1.5	30	1.2	1.5	E
14	60	0	1.5	0.6	0.7	1.5	10.	0.6	0.7	1.5	30	1.1	1.3	E
1	60	0	1.5	0.6	0.7	1.5	1.	0.6	0.7	1.5	1	0.035	0.08	SL
15	60	0	1.5	0.6	0.7	1.5	0.5	0.6	0.7	1.5	1	0.04	0.08	SL
16	60	0	0.1	0.6	0.7	1.5	1.	0.6	0.7	1.5	1	0.2	1.	SL
17	60	0.1	1.5	0.6	0.7	1.5	1.	0.6	0.7	1.5	30	0.8	2.	S
18	60	0.1	1.5	0.6	0.7	1.5	10.	0.6	0.7	1.5	30	0.8	1.3	S
						Exponents								
2	60	0	1.5	0.6	0.7	1.5	1.	0.6	0.7	1.5	5	0.17	0.28	E
19	60	0	1.5	0.6	0.7	1.5	1.	0.6	0.5	1.5	5	0.17	0.27	E
20	60	0	1.5	0.6	0.7	1.5	1.	0.6	0.7	1.	5	0.28	0.7	E
21	60	0	1.5	0.6	0.7	2	1.	0.6	0.7	1.5	5	0.16	0.21	E
22	60	0	∞	-	-	-	1.	0.6	1	1.5	5	0.13	0.22	E
23	60	0	∞	-	-	-	1.	0.6	0.7	1.5	5	0.13	0.19	E
24	60	0	∞	-	-	-	1.	0.5	0.7	1.	0	0.26	0.55	E
25	60	0	∞	-	-	-	1.	0.5	1	1.	0	0.8	1.3	E
26	60	0	∞	-	-	-	1.	0.5	2	1.	0	1	1.3	E
5	60	0	1.5	0.9	1.01	1.	∞	-	-	-	0	0.015	2.	L
27	60	0	1.5	2.	1.	1.	∞	-	-	-	0	0.17	3.3	S
10	60	0	60	2.	2.	1.	∞	-	-	-	0	2.	4.	S
						Initial Topography								
2	60	0	1.5	0.6	0.7	1.5	1.	0.6	0.7	1.5	5	0.17	0.28	E
28	60	ic	1.5	0.6	0.7	1.5	1.	0.6	0.7	1.5	5	0.	0.12	L
7	60	0	1.5	0.6	0.7	1.5	∞	-	-	-	5	0.13	0.2	E
29	60	0.1	1.5	0.6	0.7	1.5	∞	-	-	-	5	0.08	0.2	S
30	60	0.2	1.5	0.6	0.7	1.5	∞	-	-	-	5	0.01	0.14	L
1	60	0	1.5	0.6	0.7	1.5	1.	0.6	0.7	1.5	1	0.035	0.08	SL
31	60	ic	1.5	0.6	0.7	1.5	1.	0.6	0.7	1.5	1	0.	0.08	L
4	60	0	1.5	0.6	0.7	1.5	1.	0.6	0.7	1.5	30	1.55	2.1	E
17	60	0.1	1.5	0.6	0.7	1.5	1.	0.6	0.7	1.5	30	0.8	2.	S
32	60	0.2	1.5	0.6	0.7	1.5	1.	0.6	0.7	1.5	30	0.7	1.7	S
33	60	0.4	1.5	0.6	0.7	1.5	1.	0.6	0.7	1.5	30	0.5	1.7	S
34	60	0.8	1.5	0.6	0.7	1.5	1.	0.6	0.7	1.5	30	0.5	1.5	L
35	60	ic	1.5	0.6	0.7	1.5	1.	0.6	0.7	1.5	30	0.	0.6	L
25	60	0	∞	-	-	-	1.	0.5	1	1.	0	0.8	1.3	E
36	60	0.2	∞	-	-	-	1.	0.5	1	1.	0	0.15	0.7	S
37	60	0.4	∞	-	-	-	1.	0.5	1	1.	0	0.1	0.6	S
38	60	0.8	∞	-	-	-	1.	0.5	1	1.	0	0.1	0.5	S
3	60	0	1.5	0.6	0.7	1.5	1.	0.6	0.7	1.5	15	0.6	1.	E
39	60	0.4	1.5	0.6	0.7	1.5	1.	0.6	0.7	1.5	15	0.15	0.9	S
40	60	ic	1.5	0.6	0.7	1.5	1.	0.6	0.7	1.5	15	0.	0.4	L
						Saltation-Abrasion								
41[b]	60	0	1.5	0.6	0.7	1.5	10^5	0.6	0.7	-0.5	30	1.15	1.9	E

maximum possible values. First a volume eroded by nonlinear diffusion (equation (3)) is calculated. If no sediment remains, nonlinear diffusion applies to bedrock. Then, the stock of sediment available for water-driven transport is calculated by taking the sum of sediment already in the cell and the total incoming sediment. This stock is compared to the sum of transport capacities calculated for each flow pathway leaving the cell [e.g., *Thomas et al.*, 2007]. If the total transport capacity is higher than the amount of available stock, the bedrock is eroded (equation (6)), but the detached volume (the sum of detached volumes heading downstream) cannot exceed the remaining capacity. Thus, at every point in time, erosion can be limited by bedrock detachment ("detachment-limited" erosion [*Howard and Kerby*, 1983]) or by transport capacity ("transport-limited" erosion [*Willgoose et al.*, 1991a]) depending on the model's parameters and on the evolution of the topography at every point.

[16] When equation (6) is used, the sediment carried can only inhibit fluvial incision ("cover effect"). This is a useful end-member model for first-order predictions [e.g., *Seidl and Dietrich*, 1992; *Kooi and Beaumont*, 1994; *Tucker and Slingerland*, 1994, 1997], although it does not capture the various nonlinear effects of sediment [*Sklar and Dietrich*, 2006; *Gasparini et al.*, 2006, 2007]. Equation (7) is used in only one experiment in order to show that, although a more sophisticated sediment-flux-dependent erosion law can have a strong influence on the dynamic of uplifting landscapes [*Gasparini et al.*, 2006, 2007], the evolution of the mean erosion rate resulting from such a law may fall under the classification detailed in section 4.1.

[17] The finite volume approach adopted in our model (equation (8)) results in an underestimation of the river bed elevation variation. Indeed, the eroded or deposited volume is spread out over the entire cell area, which is larger than the river bed area [*Tucker and Slingerland*, 1994; *Carretier and Lucazeau*, 2005; *Loget et al.*, 2006]. Thus, with equation (8), the cell elevation is defined as the mean elevation of the cell. Alternatively, we could have calculated Δz by dividing the volume of sediment by the flow width, assuming that the cell elevation corresponds to the river bed. However, this would result in overestimating the volume gained or lost by the topography, because the river bed variation would be applied to the entire cell, even though part of the cell contains a hillslope. Consequently, the accumulated eroded volume measured from the topography would be greater than the volume measured by integrating the outflux of sediment at the mountain river outlets. Neither of these two approaches is perfect, and there has been little discussion of the differences between them.

3. Tested Parameters

[18] There are still many significant uncertainties concerning the parameters for river erosion-transport laws,

and parameter values can change in nature [e.g., *Whipple et al.*, 1998; *Tomkin et al.*, 2003; *van der Beek and Bishop*, 2003; *Whipple*, 2004]. Such variations can lead to potentially significant differences in the topographic adjustment to rock uplift [*Kooi and Beaumont*, 1996; *Davy and Crave*, 2000; *Tucker and Whipple*, 2002; *Whipple and Tucker*, 2002; *Lague et al.*, 2003; *Tucker*, 2004; *Sklar and Dietrich*, 2006; *Gasparini et al.*, 2006; *Whittaker et al.*, 2007a; *Cowie et al.*, 2008]. We carried out 41 numerical experiments in order to investigate these differences (Table 2).

[19] In one such reference experiment (E2), we must first justify the parameter values. This experiment applies to a 50×60 cell grid (cell width of 250 m), corresponding to an initial horizontal surface with Gaussian noise ($\sigma = 0.5$ m). Alluvial transport and bedrock detachment laws (equations (4) and (6)) are power functions of the excess shear stress and assume steady, uniform flow in a wide channel. Using the Manning flow resistance equation, $m = \alpha = 0.6$ and $n = \beta = 0.7$ in equations (4) and (6) [see, e.g., *Tucker*, 2004].

[20] The excess shear stress exponent of the transport capacity $p = 1.5$ and the transport coefficient $K_{all} = 1.5 \ 10^{-5}$ m^2 s^{-1} Pa$^{-1.5}$ (equation (4)) correspond to the *Meyer-Peter and Muller* [1948] formula. The value of τ_c is 5 Pa, which corresponds to grain size of about 1 cm in diameter.

[21] The excess shear stress exponent a of the bedrock incision law is set at 1.5, which lies within the expected range [1–2.5] for the abrasion processes [*Whipple et al.*, 2000]. The incision coefficient $K_{br} = 10^{-9}$ m s^{-1} Pa$^{-1.5}$ (equation (6)) is similar to previously assumed values [e.g., *Tucker and Bras*, 2000; *Tucker*, 2004; *Carretier and Lucazeau*, 2005] and leads to a fluvial slope of around 300 m/15 km.

[22] The flow width parameter $k_w = 12$ m$^{-1.5}$ s$^{0.5}$ results in a river width of about 20 m at outlet. Finally, the equation for hillslope processes uses classical values for the diffusion coefficient $\kappa = 10^{-2}$ m^2 a^{-1} [e.g., *Martin and Church* 1997] and the slope stability threshold $S_c = 0.6$ (=tan 30°) for sediment and $S_c = 1.7$ (=tan 60°) for bedrock.

[23] Our analysis focuses on the effects of the following factors (Table 2): (1) the transport threshold τ_c. The tested values (<30 Pa) correspond to grain sizes ranging between fine sand and 5 cm in diameter, (2) the system size, ranging from 15 to 37.5 km in length, and (3) the ratio between the incision and transport coefficients K_{br} and K_{all}, which partially controls the model's tendency to be either transport or detachment-limited during the transient response [*Howard*, 1980; *Whipple and Tucker*, 2002; *Cowie et al.*, 2006]. The values tested lead to a realistic mountain relief (between 200 m/15 km and 1500 m/15 km for drainage areas of about 100 km^2). Some experiments are entirely transport-limited and others are entirely detachment-limited, (4) the nonlinearity of erosion-transport laws in slope and discharge, with the parameters m, n, α, β, p and a in equations (4) and (6). The values tested for α, m, β, n, p

---

Notes to Table 2:

[a] Some reference experiments are repeated in order to facilitate the comparison with other ones. The code "ic" is for initially connected surface. These experiments start off from a dynamical equilibrium topography and a doubled uplift rate. Other values of the initial slope are measured in degrees. The unit K_{br} is m s^{-1} Pa^{-a}. $K_{br} = \infty$ means that sediments are always fully available (transport-limited). The unit K_{all} is m^2 s^{-1} Pa^{-p}. $K_{all} = \infty$ means that the transport capacity is infinite, so the volume detached from bedrock is only limited by bedrock resistance (detachment-limited). The unit τ_c is Pa. The letters for each type of model correspond to E, exponential; SL, straight line; L, linear; S, sigmoid. E5 appears twice with different m, n, and p values, which are strictly consistent and help for comparing with other experiments.

[b] *Sklar and Dietrich*'s [2004] law for bedrock incision (equation (4)); $w_f = 0.3$ m s^{-1}, $b = 1.5$.

and a are all within the expected range [0.5–2] for many bedrock erosion and transport laws [*Whipple et al.*, 1998; *Yalin*, 1972] and (5) the initial topography. The initial surfaces tested are either horizontal, gently inclined planes, or a topography equilibrium of another experiment from which the uplift rate is doubled.

[24] Experiment E41 uses the same parameters for $a = -0.5$, $b = 1.5$ (equation (7)) from *Sklar and Dietrich*'s [2004] law. The fall velocity in water, $w_f = 0.3$ m s^{-1}, corresponds to sediment grain size of several centimeters wide, and consistent with $\tau_c = 30$Pa. The detachment coefficient K_{sa} is larger (10^{-4} m^{-1}) than the value of *Sklar and Dietrich* [2004] to avoid unrealisticly large slopes for small drainage areas [see *Gasparini et al.*, 2007].

[25] All simulations use periodic boundary conditions linking the western and eastern sides of the model grid, a wall boundary (no output flux) on the north side and free output flux on the south side. The same uplift rate U (1 mm a^{-1}) and precipitation rate P [LT^{-1}] (=1 m a^{-1} in all experiments) are applied uniformly to the entire domain. Starting from a specific initial surface, the model runs until a dynamic equilibrium is reached. During the transient stage, we record the evolution of the topography and erosion rate of the whole model and of selected rivers, and compare their evolution with the erosion laws under evaluation.

4. Results

[26] In the following analysis, we use the terms "complete connectivity" or "initially connected surface" [e.g., *Davy and Crave*, 2000; *Lague et al.*, 2003]. For an initially connected surface, we designate a surface in which all cells are connected to the base level through a drainage network, which remains unchanged after the onset of uplift. Note that for a planar dipping surface, all pixels are connected to the base level, but the growth of the catchment growth then modifies the drainage network. Consequently, such a surface is not called here an initially connected surface.

4.1. Large-Scale Erosion Rates

[27] Experiments typically show two stages of the topographical adjustment, as illustrated by Figure 1 for three experiments (E30, E27, E2): the first stage takes place while the drainage system is developing, and the second includes continuing evolution of the topography toward a dynamic equilibrium. The first stage lasts for an amount of time T_{co} (connectivity time), and the total response time to achieve the dynamic equilibrium from the onset of uplift is called T. T_{co} is estimated by the time at which there are no close depressions any more in experiments starting from a horizontal surface, and by the time at which channel heads reach the northern side in experiments starting from a dipping surface. T is estimated by the time at which the average spatial erosion rate $\epsilon(t) = 0.99U$ or $\epsilon(t) = 1.01U$, depending on the experiment type.

[28] We first investigate the average spatial erosion rate $\epsilon(t)$ of the uplifting block, defined as the total sediment output flux on the southern side divided by the area of the uplifted domain. Figure 2 and Table 2 sum up the results. Four typical previously observed $\epsilon(t)$ curves can be identified, some having emerged in numerical models and others

in physical models: The first is known as the "linear"-type because it has the form of a linear response function $\epsilon(t) = U(1 - \exp(-t/T))$ [e.g., *Kooi and Beaumont* 1996]. The second characteristic $\epsilon(t)$ curve is the "sigmoid"-type. This sigmoid curve has been observed, for example, in both physical experiments [*Hasbargen and Paola*, 2000] and numerical simulations [*Carretier and Lucazeau*, 2005]. The third $\epsilon(t)$ curve is the "straight-line"-type. Finally, the fourth characteristic model is the "exponential"-type with a concave up increase of $\epsilon(t)$ and a transient maximum that is greater than the uplift rate [e.g., *Lague*, 2001]. As we examine in detail in the following, these model types depend strongly on T_{co}.

[29] Linear-type curves approximately obey an equation of the type $\partial\epsilon/\partial t = (U - \epsilon)/T$, which is the equation of a linear system with input U and output ϵ [*Kooi and Beaumont*, 1996]. Linear-type models have a negligible connectivity time T_{co} compared to T. This is pertinent for some of the experiments that start from an inclined plane (E30), all the experiments starting from a previous dynamic equilibrium that double the uplift rate, no matter what the value of τ_c is (E28, E31, E35, E40), and one transport-limited experiment that uses a threshold-free transport law linear in discharge and slope (E5). In the latter, drainage connections form between depressions on the plateau, which is similar to experiment E27 as shown in Figure 1b. This creates depressions with larger area, and their capture helps the drainage network develop quickly. Experiments that are entirely transport-limited and those including detachment-limited erosion can also be linear (e.g., E30 and E28). For experiments in which erosion can be detachment-limited, increasing the initial regional slope does not necessary imply a negligible T_{co} (e.g., E4, E17, E32, E33, E34). From a certain regional slope, T_{co} even remains constant (E33, E34 and E37, E38), which suggests that detachment-limited erosion imposes a significant connectivity time to establish the drainage network. Note that no closed depression exists in any of the experiments that starts from a dipping surface, because the regional slope dominates the gaussian noise added to initial elevations.

[30] The conditions required for a linear-type model are consistent with *Kooi and Beaumont*'s [1996] conclusions. The linear behavior of the whole system essentially requires that the drainage network does not change after the onset or acceleration of uplift. This is true for experiments starting from a previous dynamic equilibrium. For other linear-type experiments, the drainage network is established very quickly (see Figure 1a). Strictly speaking, linear behavior should be valid for erosion/transport laws linear in slope only [*Kooi and Beaumont*, 1996; *Lague*, 2001]. However, our experiments show that quasi-linear behavior can emerge from laws that incorporate a positive τ_c and that are thus nonlinear in slope (E28, E30, E35, E40). This is the case for some experiments starting from a dipping surface (E30) or from an initially connected surface (E28, E35, E40). For these experiments, the nonlinearity of erosion/transport laws is not the main factor controlling the shape of the $\epsilon(t)$ curve.

[31] Straight-line-type models combine two characteristics: (1) a significant T_{co} and (2) very low river concavities. In these models (E1, E15, E16), T_{co} is large because the drainage network development rate is limited by bedrock detachment at channel heads. However, the erosion tends to

A- Linear-type model (E30)
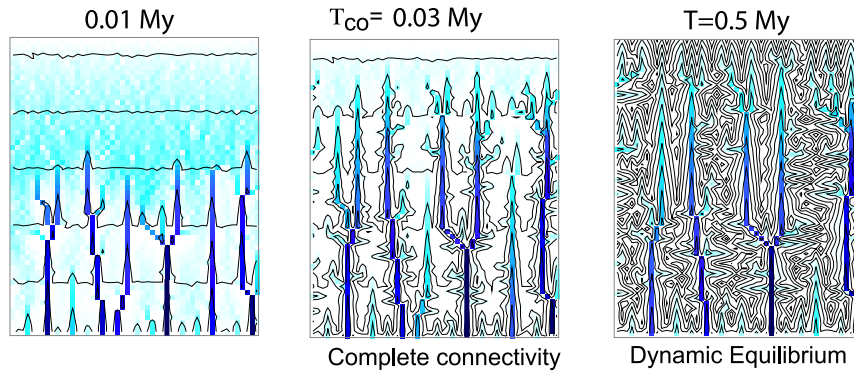
B- Sigmoid-type model (E27)
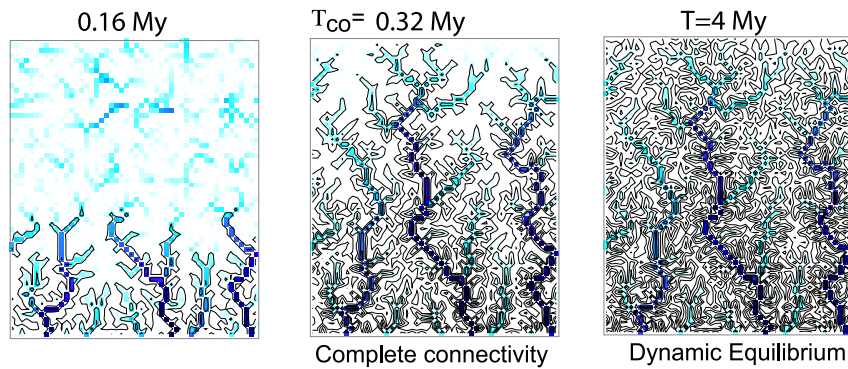
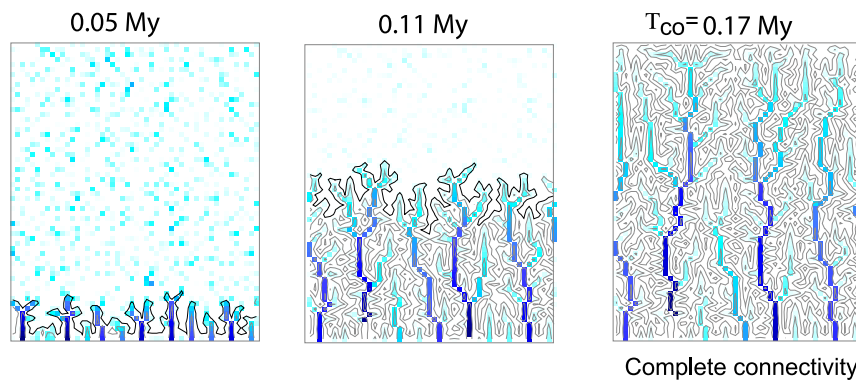## C- Exponential-type model (E2)

Figure 1. Example of the topographic evolutions. The north side is a closed boundary, the west and east sides have periodic boundaries, and the south side has an open flux and a fixed elevation boundary condition. Uplift and precipitation are constant and homogeneous. T_{co} is the connectivity time defined as the time needed for catchments to capture all the cells that belong to them when they have reached their steady state configuration. Color indicates the water flux normalized by the maximum value in the grid. The initial topography is either a surface inclined toward the south (Figure 1a) or an horizontal surface (Figures 1b and 1c) with Gaussian noise ($\sigma = 0.5$ m). (a) Linear-type model (E30). The connectivity time is negligible compared to the total response time needed to achieve dynamic equilibrium. (b) Sigmoid-type model (E27). Note that links form in the plateau which help the growth of the drainage network. Links form because of transport-limited threshold-free conditions in which $n = 1$. (c) Exponential-type model (E2). Note the long horizontal retreat during the drainage network growth. In this case, the total response time is $T = 0.28$ Ma.

A-

B-
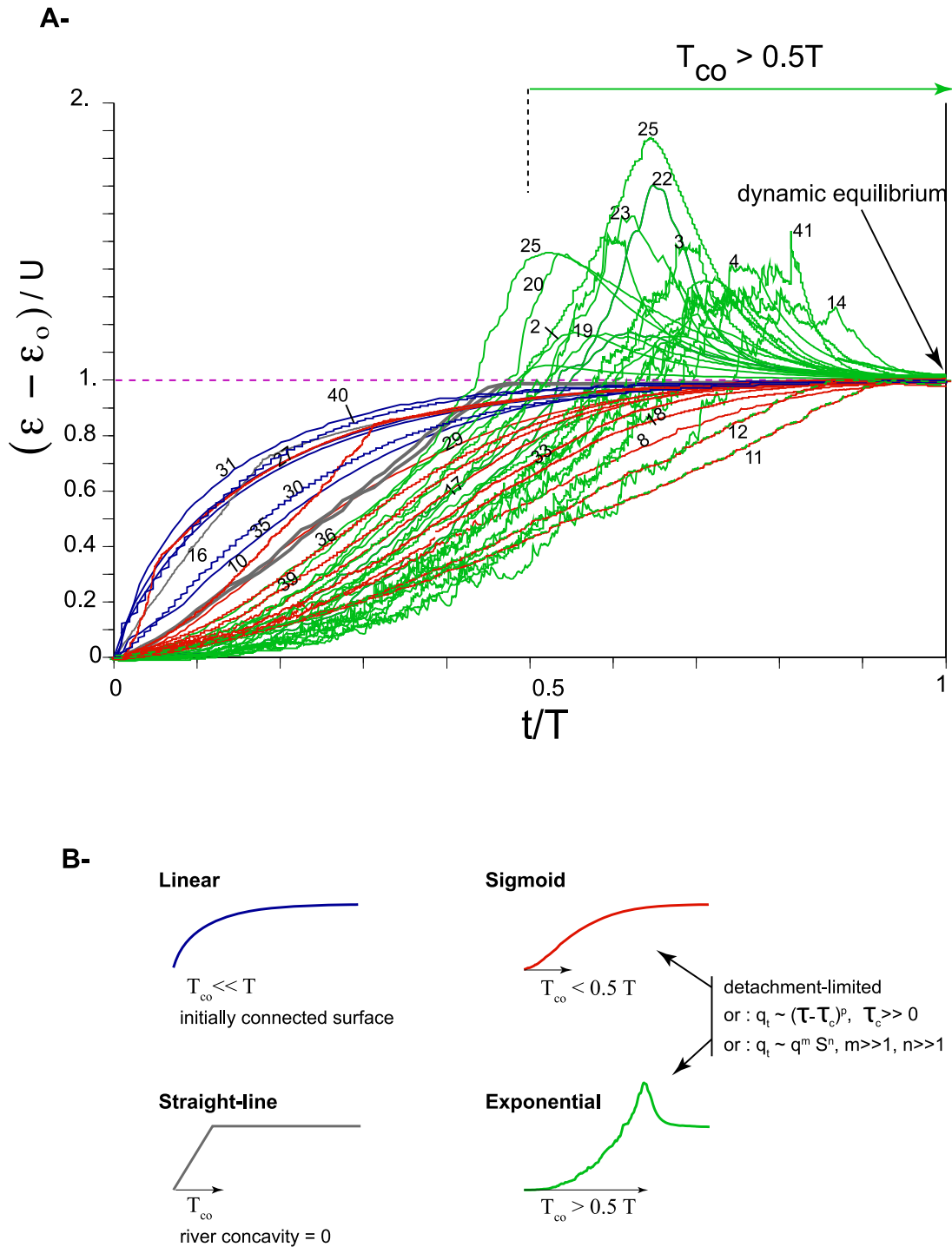
Figure 2. Plateau-scale erosion rates for various erosion laws, system sizes, and initial surfaces (see Table 2). (a) Erosion rates are normalized using the initial mean erosion rate ϵ_o (has a value other than zero for experiments that use the end of a previous experiment as their initial topography) and the uplift rate U; Time is normalized by the maximum response time T necessary to achieve dynamic equilibrium. Numbers refer to experiments (only those for which the curve is easy to see, Table 2). Irregularities arise from capture of depressions. (b) The types of models as defined by the results and the corresponding conditions needed to obtain these models.

be transport-limited at the dynamic equilibrium, so that the parameters of the transport capacity determine the river concavity. The river concavity at dynamic equilibrium is also the exponent θ in the slope-area relationship $S \propto A^{-\theta}$, obtained by equating the tectonic flux and the sediment flux (equation (A5)) [e.g., *Flint*, 1974; *Tarboton et al.*, 1989; *Willgoose et al.*, 1991b]. The parameters of the transport capacity used in straight-line-type experiments lead to a very low concavity $\theta = 0.05$ that implies a very smooth topography and straight rivers [*Kirkby*, 1971; *Tucker and Whipple*, 2002]. A concavity of 0 is generally not observed in real or experimental river profiles [*Whipple and Tucker*, 2002; *Lague et al.*, 2003] (except for those rivers that receive water only at the highest elevations). Large concavity values can be associated with significant τ_c [*Tucker*, 2004]. There is a growing number of arguments pointing to the significant effect that the transport threshold τ_c has on the erosion dynamic of mountain belts [*Parker*, 1978; *Snyder et al.*, 2003; *Talling*, 2000; *Lague et al.*, 2003]. This arguments suggest that the straight-line-type model is unrealistic. We point out that parameters of experiment E5 lead to $\theta = 0$ but E5 has a linear-type behavior. In this experiment, transport-limited erosion is imposed, contrary to the straight-line-type experiments that incorporate detachment-limited erosion. Thus, the drainage network develops very quickly in E5, which leads to a linear-type model.

[32] Sigmoid-type models are characterized by a significant T_{co} value that corresponds to the time before the inflexion point of the sigmoid curves (Figure 2). This long T_{co} implies a wave-like behavior during the connectivity phase, and a more diffusive behavior after (Figure 1b). The growth of the drainage network is responsible for the nonlinearity of the whole system's response as measured by the mean erosion rate [see also *Kooi and Beaumont*, 1996]. These models include detachment-limited experiments (E36, E37, E38), experiments using a significant $\tau_c > 1$ Pa (E17, E18, E29, E32, E33, E34), and transport-limited experiments using a threshold-free transport capacity that is more than linear in water discharge (E10, E27). The common point in these experiments, as we explain in detail in section 5.2, is that the sediment flux (the transport capacity in the transport-limited experiments or the upstream integral of detached sediment in detachment-limited experiments) increases more than linearly with water discharge. Sigmoid-type models appear to be intermediate, falling between the linear and exponential types.

[33] Exponential-type models correspond to models with a much more significant period of connectivity (typically $T_{co} > 0.5\ T$ see Figure 2), and for which the mean erosion rate passes through a maximum that is higher than the uplift rate. During the drainage network growth, $\epsilon(t)$ can be approximated by a function of the type $(e^t - 1)$ or equivalently by a power law function of t with an exponent >1. Exponential-type models result from the same kind of erosion and transport laws as the sigmoid-type models. In the case of transport-limited, threshold-free models, the transient excess of the mean erosion rate above the uplift rate is almost imperceptible (Figure 2a), even when the length of the system length is more than doubled (E11, E12). This difference is explained by (1) the intrinsically diffusive character of transport-limited erosion that limits the

rate of sediment exportation in catchments and thus prevents the mean erosion rate from significantly exceeding the uplift rate [see also *Lague*, 2001] and (2) the fact that endoreic zones get connected on the plateau, which favors the drainage network growth rate (Figure 1b). This second point is true if the value of the slope exponent n of the transport capacity law is not too much greater than 1. With higher values of n, the transport capacity decreases dramatically for very low slopes (smaller than 1) on the plateau, which prevents the development of the drainage links.

[34] In summary, quasi-linear models occur if $T_{co} = 0$, sigmoid-type models occur if $T_{co} < 0.5T$, and the exponential-type models occur if $T_{co} > 0.5T$. Figure 2b sums up the relationships between model type, associated conditions and the T_{co}/T ratio. There is not further discussion of the straight-line model, as it appears to be unrealistic.

4.2. Relationships Between Large-Scale and Local Erosion Rates and River Profile Evolution

[35] If the local incision rate in a river exceeds the uplift rate, does this imply that the mean erosion rate is of an exponential nature? Is there a relationship between the type of mean erosion rate evolution and the shape of transient river profiles? To answer these questions, we extracted the profiles of major rivers over time from each experiment, and plotted the evolution of the local incision rate for two points located on the first and second thirds of the river (P1 and P2). The results are summarized in Figure 3, which displays the large-scale mean erosion rate ϵ, the large-scale mean elevation (z), the profile adjustment of a selected river and the evolution of the incision rates (I) at these two selected points. The three cases shown in Figure 3 correspond to the experiments illustrated in Figure 1 (E30 for the linear-type, E27 for the sigmoid-type, and E2 for the exponential-type). The following differences can be observed:

[36] 1. None of the models shows a concave up increase in the mean elevation curve during the development of the drainage network. The mean elevation of the exponential-type reaches a maximum, but this occurs before the maximum of the mean erosion rate.

[37] 2. The river profiles evolve differently for each type of model. In the linear model the profile evolves by increasing the slopes. In the sigmoid-type model, the river profile evolves by first decreasing and then increasing the slopes. In the exponential-type model, the river profile evolves by decreasing the slopes.

[38] 3. In the case of the linear-type model, the local incision rates of the two points never exceed the rock uplift rate, whereas they can reach much greater values than the rock uplift rate in the two other cases. However, the time at which this local maximum occurs corresponds to the passing of a retreating erosion wave [*Stark and Stark*, 2001], and thus is not related to the time at which the maximum mean erosion rate occurs (in the exception of the points located at the catchment head). Moreover, the farther the point is located within the catchment, the more pronounced is the spike of the incision rate. This reflects the fact that disequilibrium increases toward the channel head.

[39] These relationships between the evolution of the mean erosion rate, local erosion rate and transient river profiles were observed in all our experiments. In the case of the linear-type model, the river profile can show a wave-like
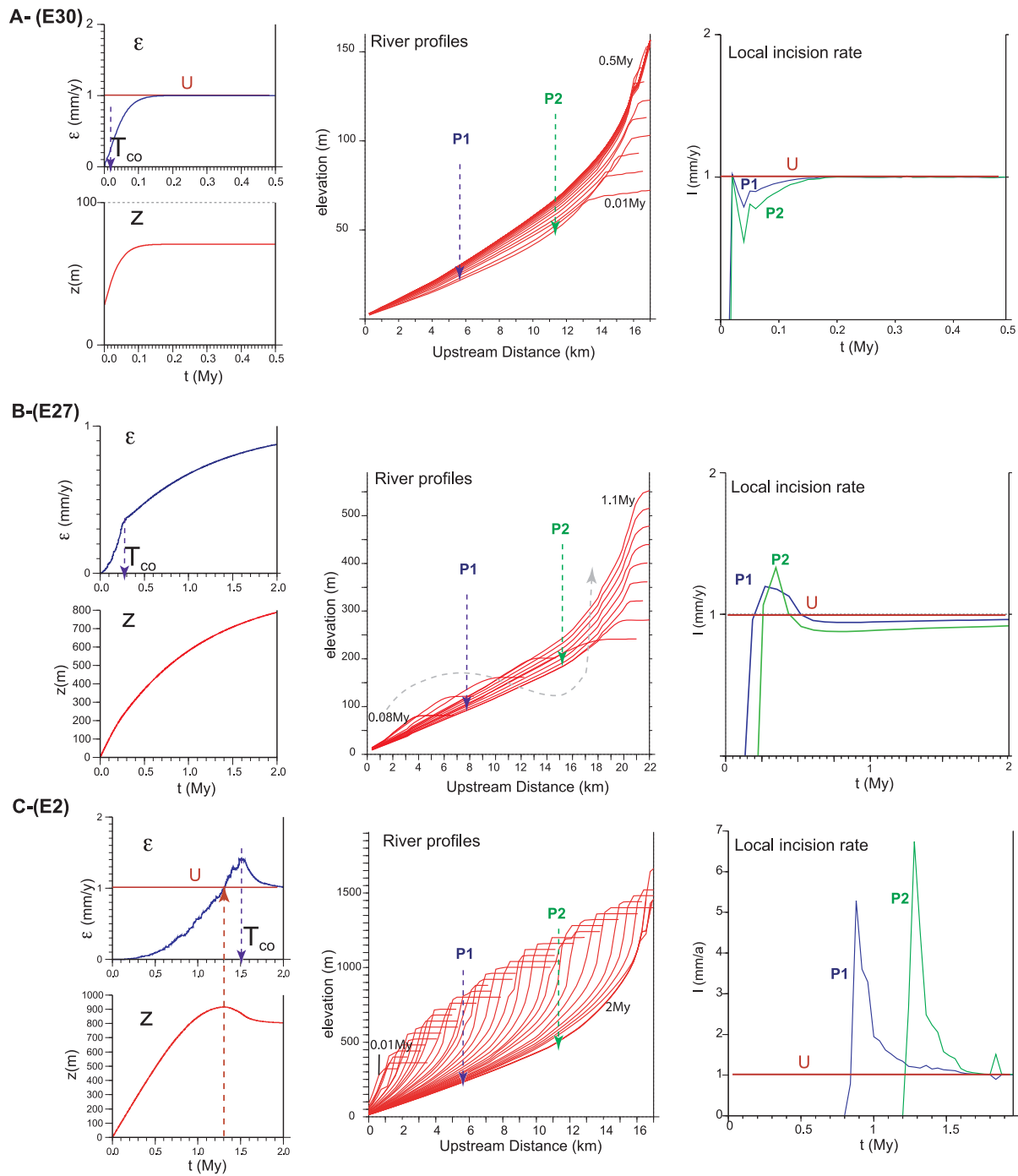
Figure 3. Relationships between large-scale mean erosion rate ϵ, mean elevation z, river profile evolution of a selected river and local river incision rates I for two selected points P1 and P2 on this river. The models correspond to Figure 1. (a) Linear-type model (E30, transport-limited erosion and dipping initial surface). The connectivity time is negligible. Note that river profiles evolve mostly by increasing their slope. The local incision rates never exceed the uplift rate. This behavior corresponds to the "downwearing" scarp evolution model. (b) Sigmoid-type model (E27, transport-limited erosion and horizontal initial surface). River profiles evolve first by decreasing and then by increasing their slopes, as underlined by the grey arrow. Local incision rates are greater and then smaller than the uplift rate. We limit the time window (dynamic equilibrium has not yet been reached) to better observe this evolution. (c) Exponential-type model (E2, transport and detachment-limited erosion). Note that the ϵ and z maximums are shifted: the z maximum arises when $\epsilon = U$, before the ϵ maximum. During the development of the drainage network, river profiles evolve by decreasing their slopes downstream from the plateau edge ("scarp retreat" scarp evolution model), and local incision rates always exceed the uplift rate.
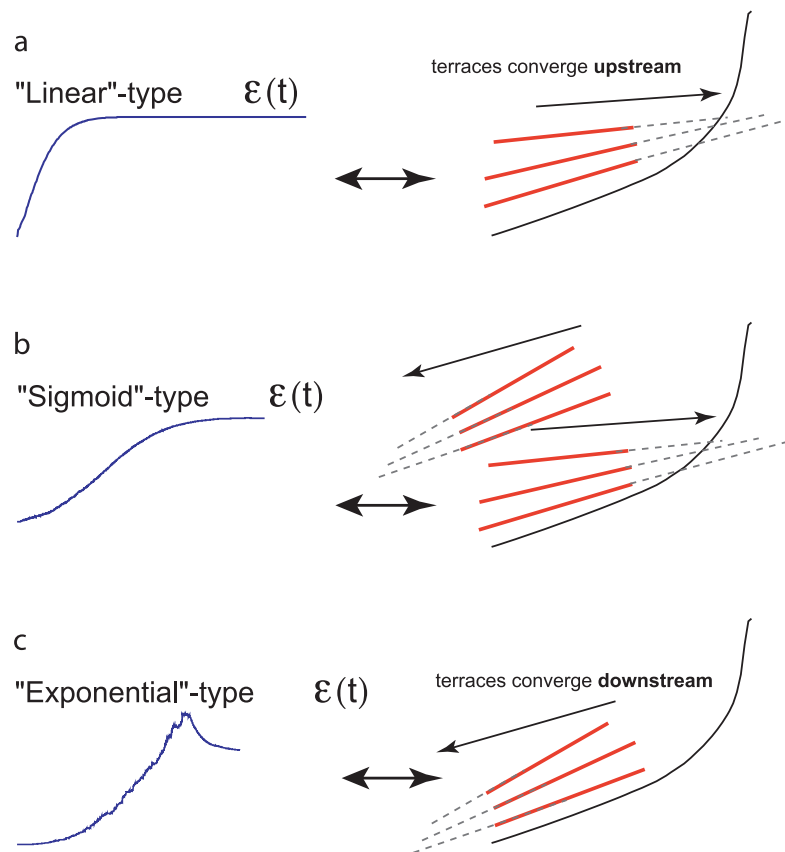
Figure 4. (left) Relationship between large-scale erosion rate evolution and (right) the geometry of the terraces for the three types of models along the river profile. (a) In the case of the linear-type model, an upstream terrace convergence is expected. (b) In the sigmoid-type model, if the connectivity time is long enough when compared to the total response time, a change in the terrace convergence is possible, with the oldest terraces converging downstream and the youngest ones upstream. (c) In the exponential case, a downstream convergence is expected. These geometric results are obtained with a homogeneous uplift pattern and a constant rate of precipitation.

behavior during its evolution, which is different from the example displayed in Figure 3a. This occurs for detachment-limited models that start from a previous equilibrium and that double the uplift rate. However, even in this case, the relationships described above remain true. So it seems that, once again, the ratio between T_{co} and T determines the style of the topographic adjustment for all scales.

[40] The difference between the shapes of the mean erosion rate and the mean-elevation curves, as well as the shift between the maximum mean erosion rate and the maximum mean elevation in the exponential-type model, can be explained rather simply. Indeed, the mean elevation z is

$$z(t) = z(0) + Ut - \int_0^t \epsilon(t')dt' \qquad (9)$$

Thus the maximum of z occurs when $dz/dt = U - \epsilon(t) = 0$, which is when the erosion rate equals the uplift rate for the first time (Figure 3).

4.3. Implication for the Field Interpretation of Terraces

[41] The three styles of river adjustment that have been identified may have implications for interpreting field data (Figure 4). If we consider that the successive river profiles correspond to terraces abandoned by climatic or sediment-driven river width variations, then the downstream or upstream convergence of terrace long profiles can be strongly influenced by the length of the connectivity phase. In linear-type models, terraces must converge upstream, while in exponential-type models terraces converge downstream. The sigmoid-type models are capable of generating terraces that converge both downstream for the oldest terraces and upstream for the youngest ones (Figure 4b). However, these predictions are made for temporally and spatially constant uplift rate and precipitation, whereas real systems can be much more complex [*Molnar et al.*, 1994; *Merritts et al.*, 1994; *Pazzaglia and Brandon*, 2001; *Poisson and Avouac*, 2004].

4.4. Application

[42] We tested the identified relationships on a well-studied field example located on the Ih Bogd Mountain, in Mongolia [*Ritz et al.*, 1995; *Bayasgalan et al.*, 1999; *Carretier et al.*, 2002; *Ritz et al.*, 2003; *Vassallo et al.*, 2005, 2007b, 2007a; *Jolivet et al.*, 2007]. The Ih Bogd Mountain is a 50×25 km^2 transpressional ridge associated with a major 260 km long strike-slip fault system. It is bounded by

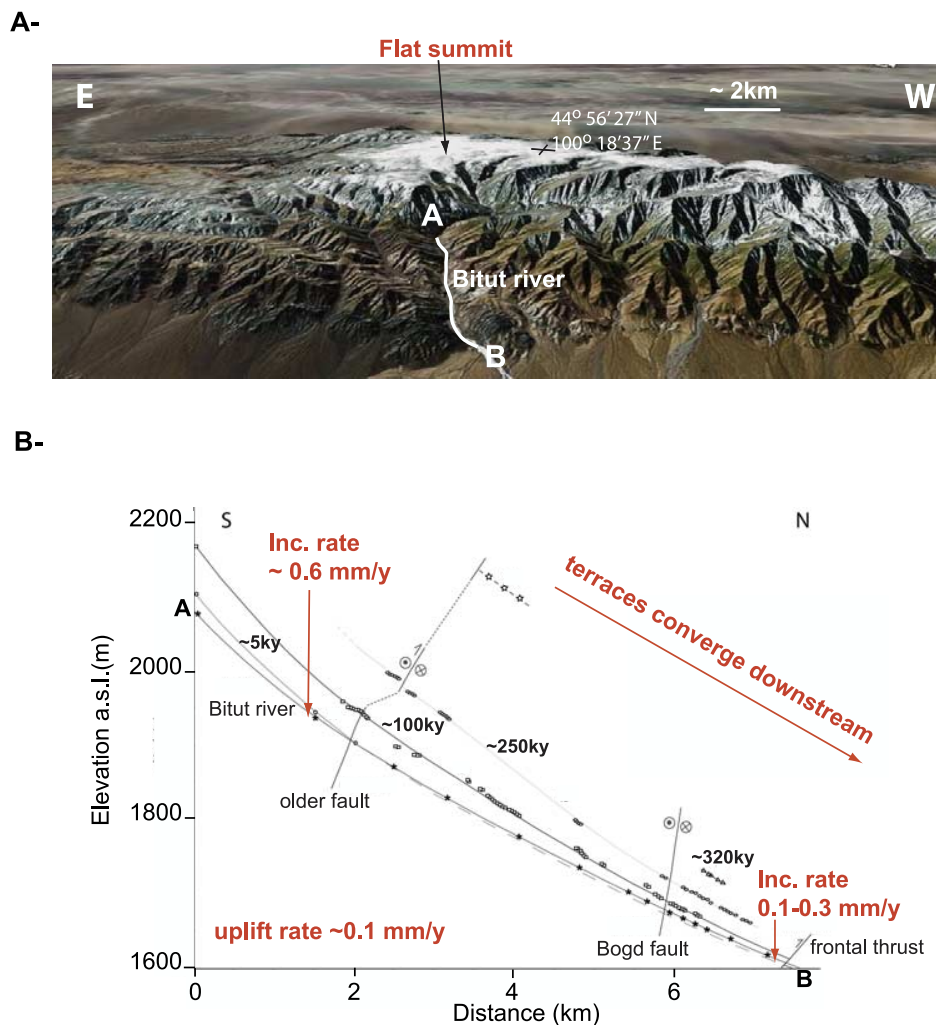**Figure 5.** (a) The Ih Bogd Mountain in Mongolia [*Vassallo et al.*, 2007b]. This is an example of a pop-up uplifting at $0.1-0.2$ mm a^{-1} during the Pleistocene. Its flat summit (image source Google Earth, used with permission) shows that the preuplift surface is not entirely connected yet. (b) Incision rates deduced from ^{10}Be dating of the Bitut river terraces show that the long-term incision rate exceeds the rock uplift rate by up to 6 times. Moreover, the terraces converge downstream. Altogether the flat summit, the fact that the incision rate is larger than the uplift rate and the downstream convergence of terraces, all suggest that this mountain is of the exponential-type. Thus its erosion rate on all scales and its river adjustments are strongly controlled by the growth of the drainage network, which supports *Vassallo et al.*'s [2007b] conclusions.

reverse fault segments. Like many other mountains in this area, Ih Bogd has conserved a large part of the undissected, preuplift surface remnant in its core [*Jolivet et al.*, 2007] (Figure 5), showing that this massif is still in the drainage growth phase ($t < T_{co}$), which is particularly long considering that uplift began about 5 Ma ago [*Vassallo et al.*, 2007a]. This surface dips very gently (<1°) toward the Bitut Valley, without any trace of channelized flow. The soil has periglacial characteristics, with a roughness of several tens of centimeters, and small (10 m x 10 m) and shallow depressions (<1 m) with desiccation traces. The evaporation and infiltration rates are unknown but possibly significant given the very low regional slope of the plateau. The drainage network is clearly retreating into the plateau, with

channel heads showing a sharp slope break [*Vassallo et al.*, 2007a]. Topographic surveys and cosmogenic nuclide dating from the Bitut river terraces allowed *Vassallo et al.* [2007a] to quantify incision rates between terraces. Dating suggests that terraces formed every 100 ka, so that the incision rate should integrate climatic variations, as assumed in our theoretical study. Independent estimates of uplift rates on bounding faults allowed [*Vassallo et al.*, 2007a] to compare the Pleistocene uplift rate (ca 0.1 mm a^{-1}) with the Pleistocene incision rates. Uplift rates for both sides of the massif are similar, and the core surface is almost horizontal, which suggests that the uplift rate is spatially constant. Incision rates are 3 to 6 times larger than the uplift rate (Figure 5), which *Vassallo et al.* [2007b] interpreted as being

mainly the result of drainage growth, and also of the interaction with piedmont and cyclic climatic variations [*Carretier and Lucazeau*, 2005]. Figure 5 shows that Bitut terraces converge downstream. This observation, along with the fact that the local incision rates are greater than the rock uplift rate and the existing remnant of the preuplift surface are all consistent with an exponential-type model. All this supports *Vassallo et al.*'s [2007] conclusions that in this case, most of the topographic adjustment to rock uplift for different scales is controlled by the ongoing growth of the drainage system. This also suggests that the long timescale erosion is either detachment-limited or transport-limited with a positive transport threshold, which seems to be consistent with the coarse sediment cover and exposed bedrock in some parts. Catchment-scale erosion rates are not yet available so it is not possible to prove the full consistency between this example and the proposed theory.

5. Discussion

5.1. Analogy With Biological Population Growth and Percolation

[43] Drainage network growth has been shown to be analogous to invasion-percolation models on the basis of similar fractal dimensions of the drainage network [*Stark*, 1991; *Yakovlev et al.*, 2005]. Moreover, *Stark* [1994] studied the relative effects of three processes and elements involved in the retreat of a drainage front: weathering and weakening of the substratum, seepage erosion and initial rock strength. To take these components into account, he used a phenomenological modeling approach based on network growth theories including invasion-percolation, diffusion-limited aggregation (DLA) and Eden growth (parallel retreat). Varying the strength of each process, he showed that the drainage front line is more or less irregular with fractal dimensions depending on the processes involved. Similar front shapes have been observed in our experiments, though varying in time and between different experiments. Such shapes include uniform retreat (Eden growth) and localized channel head invasion, although seepage erosion is not taken into account (Figure 1). In our simulation, erosion retreat proceeds either by reducing the slope to a critical slope (equation (3)), which favors Eden growth, or through fluvial erosion, depending on the transport threshold τ_c. However, bedrock collapse is not the dominant process, as model slopes are generally much smaller than S_c. In any case, just as in *Stark*'s [1994] model, network growth depends on the initial cell property (initial slope and associated drainage area) and processes that weaken the rock resistance to erosion, and which can evolve in time. The latter corresponds to the formation of drainage links on the plateau or the capture of depressions that suddenly increase the erosive power of cells located just downstream the captured depression. A visual inspection of the different shapes of the erosion front did not show a clear correlation between a particular shape and model type, in particular because the mode of channel retreat varies with time. Nevertheless, Eden growth seems to be more pronounced in sigmoid and exponential-type models, as shown in Figure 1. We did not carry out a fractal analysis due to the coarse resolution of the model grid.
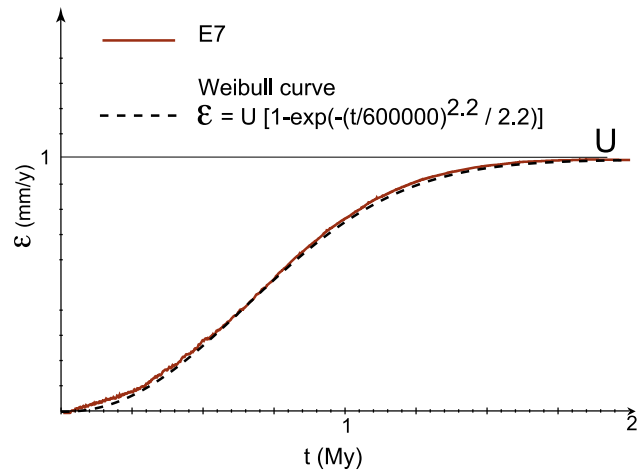

Figure 6. Weibull fit of the mean erosion rate evolution in experiment E17.

[44] Here we make another comparison. In analyzing the sigmoid-type models, it can be noted that the $\epsilon(t)$ curve follows a Weibull curve, defined as (Figure 6):

$$\epsilon(t) = U\left[1 - \exp\left(-\frac{(\gamma t)^\mu}{\mu}\right)\right] \quad (10)$$

where γ is the inverse of a characteristic time and μ is a positive constant that lies between 1 and 2.5 in our experiments. If $\mu = 1$, $\epsilon(t)$ is a linear-type model. The connectivity time T_{co} corresponds to the maximum slope of the Weibull curve, so that

$$T_{co} = \frac{(1 - \mu)^\mu}{\gamma} \quad (11)$$

[45] It is interesting to note that such sigmoid curves (Weibull, Logistic, etc..) are known in biology to represent population growth processes in a context of competition for food in a limited space, which are often modeled as percolation models. The eroded volume at each moment in time might be analogous to population growth. If this analogy is correct, then the connectivity process is limited by the potential to erode (the food), as this potential is limited by bedrock detachment or an entrainment threshold.

[46] The exponential-type models deviates from the Weibull curve. This may be due to a fundamental difference with the population analogy: in the case of an actively uplifting mountain range, the erosion rate seems to be able to make "reserves", which is to say that some material provided by rock uplift is stocked for later. This can lead the mountain to an unstable state in which its erosion rate and mean elevation are greater than the equilibrium state. This is not observed in population growth studies because populations do not usually make food reserves over long periods of time. In the case of a mountain, the potential erosion can be stocked up during the connectivity stage because slopes are abnormally large as a consequence of the small growth rate of the drainage area. When the drainage area reaches its maximum, slopes relax and the mean erosion rate decreases.
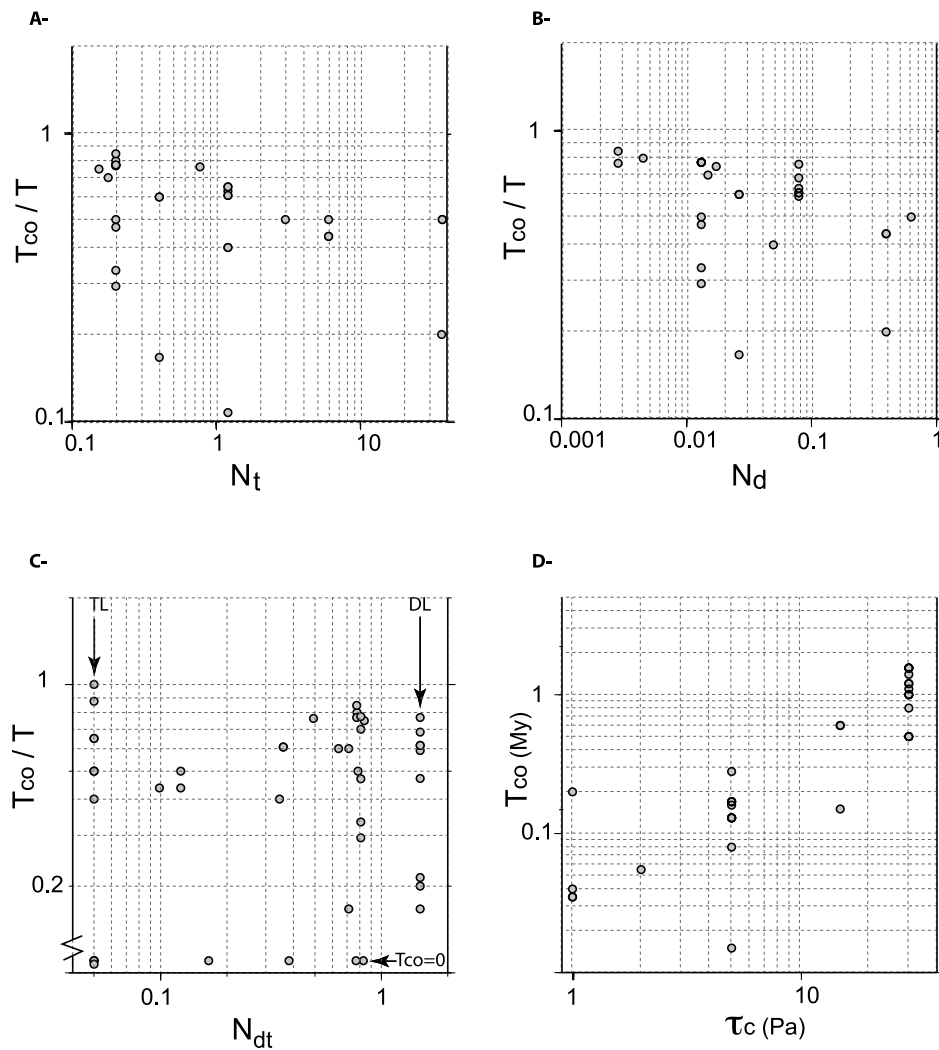
Figure 7. Attempt to find a relationship between the model's nondimensional and dimensional numbers (see Appendix A) and the ratio between the connectivity time T_{co} and the response time T or T_{co} alone. Note the log-log scale in all graphs. The capacity/competence numbers (a) N_d and (b) N_t measure the contribution of the critical entrainment stress on the equilibrium slope for the bedrock incision law and the sediment transport law, respectively. (c) The detachment/transport-limited number N_{dt} determines if erosion is detachment- (>1) or transport-limited at dynamic equilibrium. For pure detachment-limited models (DL, N_{dt} ∞) or pure transport-limited models (TL, N_{dt} = 0), an arbitrary N_{dt} value is assigned. (d) The parameter τ_c is the critical shear stress for entrainment. All these numbers are computed for a drainage area that is equal to the width of the mountain squared. Altogether, Figures 7a–7d suggest that the connectivity time increases when the sediment supply rate decreases (either by decreasing the bedrock detachment rate or by increasing the entrainment threshold), but no one of these numbers alone controls T_{co}.

5.2. What Does Limit the Drainage Network Growth?

[47] In order to study the effect of the parameters on connectivity time, we first compare the ratio between the connectivity time and the response time (T_{co}/T), or the connectivity time alone with nondimensional numbers (see Appendix A and Figure 7). Numbers N_d and N_t measure the contribution of τ_c to an equilibrium slope. They are, in other words, the ratio between the capacity to erode and the resistance (τ_c) for a specified drainage area at dynamic equilibrium, in the cases of detachment and transport-limited models, respectively [*Tucker*, 2004]. The

larger these numbers, the smaller the threshold effect. Number N_{dt} determines if the system is detachment-limited (N_{dt} > 1) or transport-limited at dynamic equilibrium for a given drainage area [*Whipple and Tucker*, 2002]. It helps evaluate the potential effect of the dominant erosion-limiting process on connectivity time. Figures 7a and 7b show that T_{co}/T tends to decrease with N_d and N_t, suggesting that τ_c increases the connectivity time significantly [see also *Lague*, 2001], which also appears when plotting T_{co} against τ_c (Figure 7d). The T_{co}/T ratio does not demonstrate a clear relationship with N_{dt}. These plots show a significant vari-

ability, suggesting that no one of the evaluated processes can explain the T_{co}/T ratio alone. Moreover, these numbers measure a balance of processes during the steady state, which may not hold during the transient stage. For example, even if transport-limited conditions are predicted at dynamic equilibrium, detachment-limited conditions can prevail in a large portion of catchments during the transient response [see also *Tucker and Whipple*, 2002].

[48] T_{co} increases linearly with the size L of the system for experiments with $\tau_c = 0$ (E8, E9, E4) and it increases as $L^{0.8}$ for experiments with $\tau_c \gg 0$ (E10, E11, E12). A more or less linear increase has also been observed in the case of threshold-free, transport-limited erosion models of an initial plateau [*Davy and Crave*, 2000], and in sandbox erosion experiments of an uplifting block [*Rohais*, 2007]. This linear increase highlights constant drainage growth rate [*Davy and Crave*, 2000]. To the contrary, *Lague et al.* [2003] observed a rate that decreased over time, but this difference could have been caused by a difference in boundary conditions: the four sides of the block are open in *Lague et al.*'s [2003] experiments, implying that the connectivity of the overall system may be limited by the competing growth of catchments that run in perpendicular directions. In the other cases, constant drainage network growth rates have been obtained for different erosion laws and initial random surfaces. This suggests that other processes control the stability of the drainage growth rate.

[49] In some cases, K_{br} influences T_{co}, and in other cases it does not. For example, T_{co} decreases with K_{br} in E4, E13, and E14 (large τ_c) and in E1 and E15 (small τ_c), but it is unchanged in E17 and E18 (positive regional slope and large threshold). In this last case, the initial dipping surface seems to control T_{co}. In the case of a small threshold case (E1 and E16), decreasing the transport capacity coefficient K_{all} strongly increases T_{co}, which confirms the intuitive notion that the rate at which sediments are evacuated influences the rate of drainage network creation. This rate depends also on the excess shear stress exponents a and p. Increasing a or p will increase the erosion/transport capacity when $\tau \gg \tau_c$, and thus enhance deep river incision or facilitate sediment exportation. This tends to decrease the connectivity time T_{co}, as illustrated by the comparison between experiments E2–E21 (p increase) and E20–E2 (a increase).

[50] The nonlinearity of erosion/transport law in discharge and slope may provide a better framework to understand how the erosion rates and topography evolutions observed in our study are controlled. In the sigmoid and exponential-type models, long T_{co} are associated with a sharp retreating front with concave-up river profiles at the channel head (Figure 3). Such a feature tends to arise under any or all the following conditions: (1) in a detachment-limited model using a stream power law with a slope exponent larger than 1 ($I \propto (Q/W)^\alpha S^\beta$, $\beta \gg 1$) [*Tucker and Whipple*, 2002], (2) in a transport-limited model using a transport law with discharge and slope exponents much larger than 1 ($qt \propto (Q/W)^m S^n$, $m \gg 1$ and $n \gg 1$), and (3) in models using erosion/transport laws that incorporate a positive threshold [*Tucker*, 2004]. As discussed in section 4.1, a slope exponent n greater than 1 limits drainage connections in the plateau and induces long T_{co}. In the case of a detachment-limited model, $\beta > 1$ creates a slope break at the plateau which prevents endoreic zones from being captured. Moreover, T_{co} significantly increases with the discharge exponents m in a transport-limited model (E5, E27) and α in a detachment-limited model (E24, E25, E26). The common point to both cases is that the volume sediment flux Q_s grows more than linearly with catchment area A (or water discharge Q) [*Smith and Bretherton*, 1972; *Tucker*, 2004], thus allowing for a deep incision in growing catchments. If this incision is large enough, hillslope gradients can increase to the point that the mean erosion rate exceeds the uplift rate [see also *Lague*, 2001].

[51] In the detachment-limited and threshold-free models ($I \propto A^{0.5}$), the rapid downstream increase of sediment flux is true by definition, because the transport capacity is implicitly assumed to be always equal or larger than the upstream integral of eroded sediment. At the river outlet, the sediment outflux Q_s is the integral of the erosion rate I over the drainage area. Therefore, Q_s is a function of A raised to a power >1. Because A increases linearly during the drainage network development, $Q_s(t)$ (or $\epsilon(t)$) at the river outlet is also a power function of t raised to a power >1. This is what is observed for the sigmoid-type and exponential-type models during the drainage network growth phase. Indeed, $\epsilon(t)$ can be approximated by a function of type $(e^t - 1)$ or equivalently by a function of type t^r with $r > 1$. In other words, the shape of the curve $Q_s(A)$ mimics the shape of the curve $\epsilon(t)$. The same relationship applies to the transport-limited and threshold-free case if $m \gg 1$.

[52] In transport-limited modes with a significant transport threshold, [*Tucker*, 2004] showed that the transport capacity increases more than linearly with the drainage area. So again, the transport law curve $Q_s = f(A)$ mimics the $\epsilon(t)$ curve during drainage growth.

[53] In addition, *Davy and Crave* [2000] found a similarity between transport-limited models in which $m \geq 2$ and detachment-limited models (laws linear in slope and with no threshold in both cases). In both cases, the characteristic time necessary to erode an initial plateau does not depend on the size of the plateau, though this is not true if $m < 2$. Also in both cases, the sediment flux is much more than linear in the drainage area, which allows for sediment to be exported over a long distance.

[54] This analysis applies to the straight-line models too. Indeed, the linear increase of the mean erosion rate corresponds to the linear scaling between the transport capacity and the water discharge.

[55] Analyzing the relationship between local erosion/transport laws and sediment outflux during drainage growth may be one way of evaluating the form that these laws take in physical models or in nature using sedimentological data. For example, [*Hasbargen and Paola*, 2000] found a more-than-linear increase of sediment outflux during the transient stage of their uplifting sandbox experiments, which is similar to the sigmoid or exponential-type models. This suggests a strongly nonlinear relationship between the erosion/transport law and water discharge. Moreover, such an increase has also been observed in reconstructed sediment outflux at Tibetan outlets [*Metivier et al.*, 1999; *Clift*, 2006]. This could correspond to our exponential-type models, although it could also correspond to temporal variations in uplift rate or climate.

[56] Other factors that have not been explored in this study are likely to exercise control over the connectivity time, such as the uplift rate [*Lague et al.*, 2003], infiltration and water sapping [*Hovius et al.*, 1998], regolith development, initial surface roughness [*Darboux et al.*, 2002], the dependence of vegetation and precipitation on altitude, the long-term decay of bedrock river width adjustment with relation to slope, discharge and carried sediment [*Finnegan et al.*, 2005; *Stark*, 2006; *Wobus et al.*, 2006; *Whittaker et al.*, 2007b; *Turowski et al.*, 2007; *Attal et al.*, 2008], the sediment-flux-dependent river incision [*Gasparini et al.*, 2007], faulting [*Sobel et al.*, 2003], etc. The relationships between these factors and the connectivity time are not clearly established in many cases. An illustrative example is the effect of the uplift rate. In their physical experiments on mountain erosion, *Lague et al.* [2003] observed no clear correlation between the rock uplift rate and the connectivity time.

[57] It is important to point out that taking the dependence of river width on slope into account, as proposed by *Finnegan et al.* [2005] and *Whittaker et al.* [2007b], is implicit in some of our experiments. In fact, the incorporation of this dependence essentially leads to the same equations (4) and (6), with a 20% to 40% larger slope exponent [*Attal et al.*, 2008]. For example, the threshold-free and detachment-limited experiments E25 and E26 use larger slope exponents than E24. A larger slope exponent tends to increase the connectivity time because, as we previously discussed, a large slope exponent prevents drainage links from forming at the channel head. This effect seems to dominate the competing acceleration of incision in gorges beneath the channel head. In the case of a normal fault acceleration, *Attal et al.* [2008] showed that a decrease in channel width with an increasing slope accelerates the topographic response. This appears to be different for an initially random surface combined with a symmetrical uplift. The effect exercised by the slope exponent can also be evaluated in the case of a significant τ_c (E22 and E23). Similar connectivity times are obtained in both cases, probably because τ_c is the key parameter controlling the nonlinear relationship between the erosion law and the slope [*Tucker*, 2004]. In addition, a significant bedrock river width adjustment time can also influence the connectivity and the entire system response time [*Stark*, 2006]. This must be evaluated further.

[58] *Gasparini et al.* [2006], *Gasparini et al.* [2007], and *Sklar et al.* [2008] showed that the use of bedrock incision models that incorporate the tool and cover effects [*Sklar and Dietrich*, 2004] significantly modifies the river profile adjustment to an increase in uplift. This can potentially yield different behaviors than those observed in our study. However, if the growth of the drainage system controls most of the system response, the behavior of sophisticated bedrock incision models might fall under the model classification that we have proposed. This is illustrated by experiment E41, which uses [*Sklar and Dietrich*'s, [2004] law and leads to an exponential-type model. The rationale could be that sediment-flux-dependent bedrock incision models converge on a transport-limited model for large drainage areas [*Gasparini et al.*, 2007]. This would mean that the nonlinearity of the transport capacity in discharge and slope may control the transient evolution of the mean

erosion rate during drainage growth. Note that *Gasparini et al.* [2006] also observed that the transient mean erosion rate exceeded the uplift rate. Nevertheless, further analysis is required to evaluate the potential effect that erosion laws incorporating tool and cover effect may have on connectivity time and the associated river profile adjustment.

[59] Finally, our hydrological model assumes that water disappears in lakes. Allowing water to fill lakes would probably decrease the drainage connectivity time, favoring linear-type rather than sigmoid or exponential-type models. However, experiments that started from a dipping surface did not contain any lakes. Significant connectivity times were observed in these cases, demonstrating that the connection of endoreic zones is not the limiting process in this case. To the contrary, the hydrological behavior of a horizontal plateau could represent a fundamental (and often neglected) controlling factor of the erosion dynamic [e.g., *Hovius et al.*, 1998].

5.3. Relation With the "Scarp Retreat" and "Down-Wearing" Scarp Evolution Models

[60] Different styles of plateau erosion have been classified in two end-member cases: the "scarp retreat" or "back-wearing," and the "down-wearing" models [*Kooi and Beaumont*, 1994; *van der Beek et al.*, 2002; *Tucker and Whipple*, 2002]. The scarp retreat model corresponds to the horizontal removal of plateau material through the propagation of an erosion wave, whereas the down-wearing model corresponds mostly to the vertical erosion of the plateau. *Tucker and Whipple* [2002] showed that these models could be strongly associated with the slope exponent in erosion law. In the case of a detachment-limited situation, if the erosion rate scales to slope with an exponent $\alpha > 1$ then scarp retreat is favored, whereas if $\alpha < 1$, down-wearing dominates. Moreover, *van der Beek et al.* [2002] showed that these two styles are also strongly influenced by the initial slope of the plateau. The existence of an inland drainage divide favors down-wearing because it allows for the rapid development of the drainage network on a surface dipping toward the base level, and erosion can occur everywhere on the plateau. To the contrary, scarp retreat occurs if the initial topography dips away from the scarp. In other words, the style of the plateau erosion is influenced by the connectivity time, which is consistent with our experiments: a dipping initial surface led to the down-wearing style and linear-type model, whereas a horizontal initial plateau implied a strongly horizontal component of erosion, associated with the sigmoid and exponential-type models (exponent, Figure 1). This suggests that the scaling of the erosion law to the slope does not necessarily control the erosion response to uplift if other factors, such as infiltration or the erosion threshold, control the connectivity. In particular, the style of plateau erosion may not be characteristic of a particular slope exponent of the erosion law if the erosion threshold is large. Indeed, a large threshold will mainly enhance the nonlinearity between the erosion rate and slope [*Snyder et al.*, 2003; *Lague et al.*, 2003; *Tucker*, 2004]. For example, experiments E22 and E23 (detachment-limited) or E2 and E19 (detachment and transport-limited) used detachment-limited erosion laws with erosion thresholds, but differ by their slope exponent. The connectivity time is the same in both pairs of experiments, showing that it is

more strongly controlled by the erosion threshold than by the slope exponents.

6. Conclusion

[61] Our study points out that the growth of the drainage network could exert a primary control over the landscape response time to uplift [see also *Kooi and Beaumont*, 1996; *Lague*, 2001; *van der Beek et al.*, 2002; *Lague et al.*, 2003]. From numerical modelings of uplifting block erosion, we have identified three main realistic model types for the evolution of the mean erosion rate. These are the linear-type, the sigmoid-type, and the exponential-type models. Linear-type models are obtained for initially connected surfaces. Sigmoid-type ($T_{co} < 0.5 \, T$) and exponential-type ($T_{co} > 0.5 \, T$) models correspond to evolutions with long connectivity times. The mean erosion rate can exceed the uplift rate in exponential-type models.

[62] Moreover, linear-type models yield river terraces that converge upstream, whereas exponential-type models yield terraces that converge downstream. Thus, by documenting the long-term sediment fluxes out of mountains and river terrace geometry, we should be able to better constrain the processes limiting erosion.

[63] In the case of the linear-type model, the local incision rate in the river never exceeds the uplift rate, in contrast to the other two cases. Thus, the large-scale erosion rate and the local incision rate could be lower or greater than the uplift rate at the same time in an uplifting block, which could explain differences in the measurements of erosion rates at different spatial scales in a catchment.

[64] Whatever the controls, connectivity time is still not totally understood, especially concerning uplift rate, sediment-flux-dependent incision and hydrology. With our model setting, long connectivity time occurs when the transport capacity is more than linear in drainage area and slope, particularly in the case of detachment-limited models, and in the transport-limited models using a positive transport threshold. To further understand what controls the connectivity time from a quantitative point of view could provide us with useful information on the erosion laws both in the real world and in physical experiments.

Appendix A: Nondimensionalization

[65] From equations (8), (4) and (6) we can write relationships between all variables at dynamic equilibrium ($\Delta z/\Delta t = 0$) for two end-members models, namely, the detachment-limited model

$$\frac{W}{\Delta x} I = U \tag{A1}$$

and the transport-limited model (all is sediment):

$$Wqt = UA \tag{A2}$$

where A [L^2] is the drainage area. Assuming no infiltration and homogeneous rainfall $Q = PA$, in both cases equilibrium slopes can be deduced as a function of A.

[66] In the detachment-limited model,

$$S_d = \left[\left(\frac{U \Delta x}{K_{br} k_w} \right)^{1/a} P^{-(0.5/a)} A^{-(0.5/a)} + \tau_c \right]^{1/\beta}$$
$$\cdot \, P^{-0.5(\alpha/\beta)} k_w^{\alpha/\beta} k_t^{-(1/\beta)} A^{-0.5(\alpha/\beta)} \tag{A3}$$

where S_d is the detachment-limited equilibrium slope. In parentheses both terms of the sum represent what *Tucker* [2004] named the capacity and competence terms, respectively. Dividing the first term by the second leads to a nondimensional number N_d, the detachment/competence number that measures the ratio between the capacity to erode and the resistance of the bedrock [*Tucker*, 2004]:

$$N_d = \frac{(U \Delta x / K_{br} k_w)^{1/a} P^{-(0.5/a)} A^{-(0.5/a)}}{\tau_c} \tag{A4}$$

[67] Similarly, from equation (A2) we obtain the following for the transport-limited model:

$$S_t = \left[\left(\frac{U}{K_{all} k_w} \right)^{1/p} P^{-(0.5/p)} A^{0.5/p} + \tau_c \right]^{1/n}$$
$$\cdot \, P^{-0.5(m/n)} k_w^{m/n} k_t^{-\frac{1}{n}} A^{-0.5(m/n)} \tag{A5}$$

where S_t is the equilibrium slope, and

$$N_t = \frac{(U/K_{all} k_w)^{1/p} P^{-(0.5/p)} A^{0.5/p}}{\tau_c} \tag{A6}$$

where N_t is the capacity/competence number for transport.

[68] Dividing S_d by S_t we obtain another nondimensional number N_{dt} the value of which determines if the erosion is transport ($N_{dt} < 1$) or detachment limited ($N_{dt} > 1$) at equilibrium as a function of the drainage area A [*Whipple and Tucker*, 2002]:

$$N_{dt} = \frac{\left[\left(\frac{U \Delta x}{K_{br} k_w} \right)^{-(1/a)} P^{-(0.5/a)} A^{-(0.5/a)} + \tau_c \right]^{1/\beta}}{\left[\left(\frac{U}{K_{all} k_w} \right)^{1/p} P^{-(0.5/p)} A^{0.5/p} + \tau_c \right]^{1/n}}$$
$$\cdot \, P^{0.5(m/n - \alpha/\beta)} k_w^{(\alpha/\beta - m/n)} k_t^{1/n - 1/\beta} A^{0.5(m/n - \alpha/\beta)} \tag{A7}$$

References

Anderson, R. S. (1994), Evolution of the Santa Cruz Mountains, California, through tectonic growth and geomorphic decay, *J. Geophys. Res.*, 99(B10), 20,161–20,179, doi:10.1029/94JB00713.

Attal, M., G. E. Tucker, A. C. Whittaker, P. A. Cowie, and G. P. Roberts (2008), Modeling fluvial incision and transient landscape evolution: Influence of dynamic channel adjustment, *J. Geophys. Res.*, 113, F03013, doi:10.1029/2007JF000893.

Bayasgalan, A., J. Jackson, J.-F. Ritz, and S. Carretier (1999), Forebergs, flower structures, and the development of large intra-continental strike-slip faults: The Gurvan Bogd fault system in Mongolia, *J. Struct. Geol.*, 21, 1285–1302, doi:10.1016/S0191-8141(99)00064-4.

Carretier, S., and F. Lucazeau (2005), How does alluvial sedimentation at range fronts modify the erosional dynamics of mountain catchments?, *Basin Res.*, 17, 361–381, doi:10.1111/j.1365-2117.2005.00270.x.

Carretier, S., J.-F. Ritz, J. Jackson, and A. Bayasgalan (2002), Morphological dating of cumulative reverse fault scarps: Examples from the Gurvan Bogd fault system, Mongolia, *Geophys J Int.*, 148, 256–277, doi:10.1046/j.1365-246X.2002.01599.x.

Clift, P. D. (2006), Controls on the erosion of Cenozoic Asia and the flux of clastic sediment to the ocean, *Earth Planet. Sci. Lett.*, 241, 571–580, doi:10.1016/j.epsl.2005.11.02.

Cowie, P. A., M. Attal, G. E. Tucker, A. C. Whittaker, M. Naylor, A. Ganas, and G. P. Roberts (2006), Investigating the surface process response to fault interaction and linkage using a numerical modelling approach, *Basin Res.*, 18, 231–266, doi:10.1111/j.1365-2117.2006.00298.x.

Cowie, P. A., A. Whittaker, M. Attal, G. Roberts, G. E. Tucker, and A. Ganas (2008), New constraints on sediment-flux–dependent river incision: Implications for extracting tectonic signals from river profiles, *Geology*, 36(7), 535–538, doi:10.1130/G24681A.1.

Darboux, F., C. Gascuel-Odoux, and P. Davy (2002), Effects of surface water storage by soil roughness on overland-flow generation, *Earth Surf. Processes Landforms*, 27(3), 223–233, doi:10.1002/esp.313.

Davy, P., and A. Crave (2000), Upscaling local-scale transport processes in large-scale relief dynamics, *Phys. Chem. Earth*, 25, 533–541, doi:10.1016/S1464-1895(00)00082-X.

Densmore, A. L., M. A. Ellis, and R. S. Anderson (1998), Landsliding and the evolution of normal-fault-bounded mountains, *J. Geophys. Res.*, 103(B7), 15,203–15,219.

Farías, M., R. Charrier, S. Carretier, J. Martinod, A. Fock, D. Campbell, J. Cáceres, and D. Comte (2008), Late Miocene high and rapid surface uplift and its erosional response in the Andes of central Chile (33°–35°S), *Tectonics*, 27, TC1005, doi:10.1029/2006TC002046.

Finnegan, N., G. Roe, D. R. Montgomery, and B. Hallet (2005), Controls on the channel width of rivers: Implications for modeling fluvial incision of bedrock, *Geology*, 33, 229–232, doi:10.1130/G21171.1.

Flint, J. J. (1974), Stream gradient as a function of order, magnitude, and discharge, *Water. Resour. Res.*, 10, 969–973.

Gasparini, N. M., R. L. Bras, and K. Whipple (2006), Numerical modeling of non–steady-state river profile evolution using a sediment-flux-dependent incision model, in *Tectonics, Climate, and Landscape Evolution*, edited by S. Willet, N. Hovius, M. Brandon, and D. Fisher, *Spec. Pap. Geol. Soc. Am.*, 398, 127–141, doi:10.1130/2006.2398(08).

Gasparini, N. M., K. X. Whipple, and R. L. Bras (2007), Predictions of steady state and transient landscape morphology using sediment-flux-dependent river incision models, *J. Geophys. Res.*, 112, F03S09, doi:10.1029/2006JF000567.

Hasbargen, L. E., and C. Paola (2000), Landscape instability in an experimental drainage basin, *Geology*, 28, 1067–1070, doi:10.1130/0091-7613(2000)28.

Hovius, N., C. P. Stark, M. A. Tutton, and L. D. Abbott (1998), Landslide-driven drainage network evolution in a pre-steady-state mountain belt: Finisterre Mountains, Papua New Guinea, *Geology*, 26, 1071–1074, doi:10.1130/0091-7613(1998)026.

Howard, A. D. (1980), Thresholds in river regime, in *The Concept of Geomorphic Thresholds*, edited by D. Coates and J. Vitek, pp. 227–258, Allen and Unwin, Boston, Mass.

Howard, A. D. (1997), Badland morphology and evolution: interpretation using a simulation model, *Earth Surf. Processes Landforms*, 22, 211–227, doi:10.1002/(SICI)1096-9837(199703)22:3<211::AID-ESP749>3.0.CO;2-E.

Howard, A. D., and G. Kerby (1983), Channel changes in badlands, *Geol. Soc. Am. Bull.*, 94, 739–752.

Howard, A. D., W. E. Dietrich, and M. A. Seidl (1994), Modeling fluvial erosion on regional to continental scales, *J. Geophys. Res.*, 99, 13,971–13,986, doi:10.1029/94JB00744.

Hurtrez, J.-E., F. Lucazeau, J. Lavé, and J.-P. Avouac (1999), Investigation of the relationships between basin morphology, tectonic uplift, and denudation from the study of an active fold belt in the Silawik hills, central Nepal, *J. Geophys. Res.*, 104(B6), 12,779–12,796.

Jolivet, M., et al. (2007), Mongolian summits: An uplifted, flat, old but still preserved erosion surface, *Geology*, 35, 871–874, doi:10.1130/G23758A.1.

Kirchner, J. W., R. Finkel, C. Riebe, D. Granger, J. Clayton, J. King, and W. Megahan (2001), Mountain erosion over 10 yr, 10 k.y., and 10 m.y. time scales, *Geology*, 29, 591–594, doi:10.1130/0091-7613(2001)029<0591:MEOYKY>2.0.CO;2.

Kirkby, M. (1971), Hillslope process-response models based on the continuity equation, *Inst. Brit. Geogr. Spec. Publ.*, 3, 15–30.

Kooi, H., and C. Beaumont (1994), Escarpment evolution on high-elevation rifted margins: Insights derived from a surface processes model that combines diffusion, advection, and reaction, *J. Geophys. Res.*, 99, 12,191–12,209, doi:10.1029/94JB00047.

Kooi, H., and C. Beaumont (1996), Large-scale geomorphology: Classical concepts reconciled and integrated with contemporary ideas via a surface processes model, *J. Geophys. Res.*, 101(B2), 3361–3386.

Lague, D. (2001), Dynamique de l'érosion continentale aux grandes échelles de temps et d'espace: Modélisation expérimentale, numérique et théorique, Ph.D. thesis, Univ. de Rennes, Rennes, France.

Lague, D., A. Crave, and P. Davy (2003), Laboratory experiments simulating the geomorphic response to tectonic uplift, *J. Geophys. Res.*, 108(B1), 2008, doi:10.1029/2002JB001785.

Lavé, J., and J. P. Avouac (2000), Active folding of fluvial terraces across the Siwaliks Hills, Himalayas of central Nepal, *J. Geophys. Res.*, 105(B3), 5735–5770.

Lavé, J., and J. P. Avouac (2001), Fluvial incision and tectonic uplift across the Himalayas of central Nepal, *J. Geophys. Res.*, 106(B11), 26,561–26,591.

Loget, N., P. Davy, and J. Van Den Driessche (2006), Mesoscale fluvial erosion parameters deduced from modeling the Mediterranean sea level drop during the Messinian (late Miocene), *J. Geophys. Res.*, 111, F03005, doi:10.1029/2005JF000387.

Martin, Y., and M. Church (1997), Diffusion in landscape development models: On the nature of basic transport relations, *Earth Surf. Processes Landforms*, 22, 273–279, doi:10.1002/(SICI)1096-9837(199703)22:3<273::AID-ESP755>3.0.CO;2-D.

Merritts, D. J., K. R. Vincent, and E. E. Wohl (1994), Long river profiles, tectonism, and eustasy: A guide to interpreting fluvial terraces, *J. Geophys. Res.*, 99(B7), 14,031–14,050, doi:10.1029/94JB00857.

Metivier, F., Y. Gaudemer, P. Tapponnier, and M. Klein (1999), Mass accumulation rates in Asia during the Cenozoic, *Geophys J Int.*, 137(2), 280–318, doi:10.1046/j.1365-246X.1999.00802.x.

Meyer-Peter, E., and R. Müller (1948), Formulas for bed-load transport, in *Proceedings of the 2nd Meeting of the International Association for Hydraulic Structures Research*, pp. 39–64, Int. Assoc. of Hydraul. Struct. Res., Delft, Netherlands.

Molnar, P., et al. (1994), Quaternary climate change and the formation of river terraces across growing anticlines on the north flank of the Tien Shan, China, *J. Geol.*, 102, 583–602.

Murray, A. B., and C. Paola (1997), Properties of a cellular braided-stream model, *Earth Surf. Processes Landforms*, 22, 1001–1025, doi:10.1002/(SICI)1096-9837(199711)22:11<1001::AID-ESP798>3.0.CO;2-O.

Nicholas, A., and T. Quine (2007), Crossing the divide: Representation of channels and processes in reduced-complexity river models at reach and landscape scales, *Geomorphology*, 90, 38–339, doi:10.1016/j.geomorph.2006.10.026.

Parker, G. (1978), Self-formed straight rivers with equilibrium banks and mobile bed. Part 1. The sand-silt river, *J. Fluid Mech.*, 89, 109–125, doi:10.1017/S0022112078002499.

Pazzaglia, F. J., and M. T. Brandon (2001), A fluvial record of long-term steady-state uplift and erosion across the Cascadia forearc high, western Washington State, *Am. J. Sci.*, 301, 385–431.

Pazzaglia, F. J., F. J. Gardner, and D. J. Merritts (1998), Bedrock fluvial incision and longitudinal profile development over geologic time scales determined by fluvial terraces, in *Rivers Over Rock*, *Geophys. Monogr. Ser.*, vol. 107, edited by K. Tinkler and E. Wohl, pp. 207–235, AGU, Washington, D. C.

Pelletier, J. D. (2004), Persistent drainage migration in a numerical landscape evolution model, *Geophys. Res. Lett.*, 31, L20501, doi:10.1029/2004GL020802.

Poisson, B., and J.-P. Avouac (2004), Holocene Hydrological changes inferred from alluvial stream entrenchment in North Tian Shan (northwestern China), *J. Geol.*, 112, 231–249, doi:0022-1376/2004/11202-0006..

Ritz, J.-F., E. T. Brown, D. L. Bourlès, H. Philip, A. Schlupp, G. M. Raisbeck, F. Yiou, and B. Enkhtuvshin (1995), Slip rates along active faults estimated with cosmic-ray-exposure dates: Application to the Bogd fault, Gobi-Altai, Mongolia, *Geology*, 23, 1019–1022.

Ritz, J.-F., et al. (2003), Late Pleistocene to Holocene slip rates for the Gurvan Bulag thrust fault (Gobi-Altay, Mongolia) estimated with [10]Be dates, *J. Geophys. Res.*, 108(B3), 2162, doi:10.1029/2001JB000553.

Roering, J. J., J. W. Kirchner, and W. E. Dietrich (1999), Evidence for nonlinear, diffusive sediment transport on hillslopes and implications for landscape morphology, *Water Resour. Res.*, 35(3), 853–870.

Rohais, S. (2007), Architecture stratigraphique et flux sédimentaires sur la marge sud du golfe de Corinthe (Grèce): Analyse de terrain, modélisations expérimentales et numériques, Ph.D. thesis, Univ. de Rennes 1, Rennes, France.

Seidl, M. A., and W. E. Dietrich (1992), The problem of channel erosion in bedrock, *Catena Suppl.*, 23, 101–124.

Sklar, L. S., and W. E. Dietrich (2004), A mechanistic model for river incision into bedrock by saltating bed load, *Water Resour. Res.*, *40*, W06301, doi:10.1029/2003WR002496.

Sklar, L. S., and W. E. Dietrich (2006), The role of sediment in controlling steady-state bedrock channel slope: Implications of the saltation-abrasion incision model, *Geomorphology*, *82*, 58–83, doi:10.1016/j.geomorph.2005.08.019.

Sklar, L., B. Dietrich, and E. William (2008), Implications of the saltation-abrasion bedrock incision model for steady-state river longitudinal profile relief and concavity, *Earth Surf. Processes Landforms*, *33*(7), 1129–1151, doi:10.1002/esp.1689.

Smith, T. R., and F. P. Bretherton (1972), Stability and the conservation of mass in drainage basin evolution, *Water Resour. Res.*, *8*(6), 1506–1529, doi:10.1029/WR008i006p01506.

Snyder, N. P., K. X. Whipple, G. E. Tucker, and D. J. Merritts (2003), Importance of a stochastic distribution of floods and erosion thresholds in the bedrock river incision problem, *J. Geophys. Res.*, *108*(B2), 2117, doi:10.1029/2001JB001655.

Sobel, E. R., G. E. Hilley, and M. R. Strecker (2003), Formation of internally drained contractional basins by aridity-limited bedrock incision, *J. Geophys. Res.*, *108*(B7), 2344, doi:10.1029/2002JB001883.

Stark, C. P. (1991), An invasion percolation model of network evolution, *Nature*, *352*, 423–424.

Stark, C. P. (1994), Cluster growth modeling of plateau erosion, *J. Geophys. Res.*, *99*, 13,957–13,969.

Stark, C. P. (2006), A self-regulating model of bedrock river channel geometry, *Geophys. Res. Lett.*, *33*, L04402, doi:10.1029/2005GL023193.

Stark, C. P., and G. J. Stark (2001), A channelization model of landscape evolution, *Am. J. Sci.*, *301*, 486–512.

Stolar, D., G. Roe, and S. Willett (2007a), Controls on the patterns of topography and erosion rate in a critical orogen, *J. Geophys. Res.*, *112*, F04002, doi:10.1029/2006JF000713.

Stolar, D., S. Willett, and D. Montgomery (2007b), Characterization of topographic steady state in Taiwan, *Earth Planet. Sci. Lett.*, *261*, 421–431, doi:10.1016/j.epsl.2007.07.045.

Talling, P. J. (2000), Self-organization of river networks to threshold states, *Water Resour. Res.*, *36*(4), 1119–1128, doi:10.1029/1999WR900339.

Tarboton, D. G., R. L. Bras, and I. Rodriguez-Iturbe (1989), Scaling and Elevation in River Networks, *Water Resour. Res.*, *25*(9), 2037–2051, doi:10.1029/WR025i009p02037.

Thomas, R., A. Nicholas, and T. Quine (2007), Cellular modelling as a tool for interpreting historic braided river evolution, *Geomorphology*, *90*, 302–317, doi:10.1016/j.geomorph.2006.10.025.

Tomkin, J. H., M. T. Brandon, F. J. Pazzaglia, J. R. Barbour, and S. D. Willett (2003), Quantitative testing of bedrock incision models for the Clearwater River, NW Washington State, *J. Geophys. Res.*, *108*(B6), 2308, doi:10.1029/2001JB000862.

Tucker, G. E. (2004), Drainage basin sensitivity to tectonic and climatic forcing: Implications of a stochastic model for the role of entrainment and erosion thresholds, *Earth Surf. Processes Landforms*, *29*, 185–205, doi:10.1002/esp.1020.

Tucker, G. E., and R. L. Bras (2000), A stochastic approach to modeling the role of rainfall variability in drainage basin evolution, *Water Resour. Res.*, *36*(7), 1953–1964, doi:10.1029/2000WR900065.

Tucker, G. E., and R. L. Slingerland (1994), Erosional dynamics, flexural isostasy, and long-lived escarpments: A numerical modeling study, *J. Geophys. Res.*, *99*(B6), 12,229–12,243, doi:10.1029/94JB00320.

Tucker, G. E., and R. Slingerland (1997), Drainage basin responses to climate change, *Water Resour. Res.*, *33*(8), 2031–2047, doi:10.1029/97WR00409.

Tucker, G. E., and K. X. Whipple (2002), Topographic outcomes predicted by stream erosion models: Sensitivity analysis and intermodel comparison, *J. Geophys. Res.*, *107*(B9), 2179, doi:10.1029/2001JB000162.

Tucker, G. E., S. T. Lancaster, N. M. Gasparini, R. R. Bras, and S. M. Rybarczyk (2001), An object-oriented framework for distributed hydrologic and geomorphic modeling using triangulated irregular networks, *Comput. Geosci.*, *27*, 959–973, doi:10.1016/S0098-3004(00)00134-5.

Turowski, J. M., D. Lague, and N. Hovius (2007), Cover effect in bedrock abrasion: A new derivation and its implications for the modeling of bedrock channel morphology, *J. Geophys. Res.*, *112*, F04006, doi:10.1029/2006JF000697.

van der Beek, P., and P. Bishop (2003), Cenozoic river profile development in the Upper Lachlan catchment (SE Australia) as a test of quantitative fluvial incision models, *J. Geophys. Res.*, *108*(B6), 2309, doi:10.1029/2002JB002125.

van der Beek, P., M. A. Summerfield, J. Braun, R. W. Brown, and A. Fleming (2002), Modeling postbreakup landscape development and denudational history across the southeast African (Drakensberg Escarpment) margin, *J. Geophys. Res.*, *107*(B12), 2351, doi:10.1029/2001JB000744.

Vassallo, R., J.-F. Ritz, R. Braucher, and S. Carretier (2005), Dating faulted alluvial fans with cosmogenic ^{10}Be in the Gurvan Bogd mountain range (Gobi-Altay, Mongolia): climatic and tectonic implications, *Terra Nova*, *17*, 278–285, doi:10.1111/j.1365-3121.2005.00612.x.

Vassallo, R., M. Jolivet, J. Ritz, R. Braucher, C. Larroque, C. Sue, M. Todbileg, and D. Javkhlanbold (2007a), Uplift age and rates of the Gurvan Bogd system (Gobi-Altay) by apatite fission track analysis, *Earth Planet. Sci. Lett.*, *259*(1–3), 333–346, doi:10.1016/j.epsl.2007.04.047.

Vassallo, R., et al. (2007b), Transpressional tectonics and stream terraces of the Gobi-Altay, Mongolia, *Tectonics*, *26*, TC5013, doi:10.1029/2006TC002081.

von Blanckenburg, F. (2005), The control mechanisms of erosion and weathering at basin scale from cosmogenic nuclides in river sediment, *Earth Planet. Sci. Lett.*, *237*, 462–479, doi:10.1016/j.epsl.2005.06.030.

Whipple, K. X. (2004), Bedrock rivers and the geomorphology of active orogens, *Annu. Rev. Earth Planet. Sci.*, *32*, 151–185, doi:10.1146/annurev.earth.32.101802.120356.

Whipple, K. X., and G. E. Tucker (1999), Dynamics of the stream-power river incision model: Implications for height limits of mountain ranges, landscape response timescales, and research needs, *J. Geophys. Res.*, *104*(B8), 17,661–17,674.

Whipple, K. X., and G. E. Tucker (2002), Implications of sediment-flux-dependent river incision models for landscape evolution, *J. Geophys. Res.*, *107*(B2), 2039, doi:10.1029/2000JB000044.

Whipple, K. X., G. Parker, C. Paola, and D. Mohrig (1998), Channel dynamics, sediment transport, and the slope of alluvial fans: Experimental study, *J. Geol.*, *106*, 667–693.

Whipple, K. X., G. S. Hancock, and R. S. Anderson (2000), River incision into bedrock: Mechanics and relative efficacy of plucking, abrasion and cavitation, *Geol. Soc. Am. Bull.*, *112*, 490–503, doi:10.1130/0016-7606(2000)112<490:RIIBMA>2.0.CO;2.

Whittaker, A. C., P. A. Cowie, M. Attal, G. E. Tucker, and G. P. Roberts (2007a), Contrasting transient and steady-state rivers crossing active normal faults: new field observations from the Central Apennines, Italy, *Basin Res.*, *19*(4), 529–556, doi:10.1111/j.1365-2117.2007.00337.x.

Whittaker, A. C., P. A. Cowie, M. Attal, G. E. Tucker, and G. P. Roberts (2007b), Bedrock channel adjustment to tectonic forcing: Implications for predicting river incision rates, *Geology*, *35*(2), 103–106, doi:10.1130/G20738.1.

Willett, S. (1999), Orogeny and orography: The effects of erosion on the structure of mountain belts, *J. Geophys. Res.*, *104*(B12), 28,957–28,981, doi:10.1029/1999JB900248.

Willgoose, G., R. L. Bras, and I. Rogdriguez-Iturbe (1991a), Result from a new model of river basin evolution, *Earth Surf. Processes Landforms*, *16*, 237–254, doi:10.1002/esp.3290160305.

Willgoose, G., R. L. Bras, and I. Rodriguez-Iturbe (1991b), A Physical explanation of an observed link area-slope relationship, *Water Resour. Res.*, *27*(7), 1697–1702, doi:10.1029/91WR00937.

Wobus, C. W., G. E. Tucker, and R. S. Anderson (2006), Self-formed bedrock channels, *Geophys. Res. Lett.*, *33*, L18408, doi:10.1029/2006GL027182.

Yakovlev, G., W. Newman, D. Turcotte, and A. Gabrielov (2005), An inverse cascade model for self-organized complexity and natural hazards, *Geophys. J. Int.*, *163*(2), 433–442, doi:10.1111/j.1365-246X.2005.02717.x.

Yalin, M. S. (1972), *Mechanics of Sediment Transport*, 289 pp., Pergamon, Oxford, U. K.

Zaprowski, B. J., F. J. Pazzaglia, and E. B. Evenson (2005), Climatic influences on profile concavity and river incision, *J. Geophys. Res.*, *110*, F03004, doi:10.1029/2004JF000138.

───────────────

S. Carretier and E. Pepin, Laboratoire de Mécanismes et Transferts en Geologie, IRD, CNRS, Université de Toulouse, 19 avenue E Berlin, F-31400 Toulouse, France. (carretie@lmtg.obs-mip.fr)

M. Farias, Departamento de Geologia, Universidad de Chile, Plaza Ercilla 803, Box 13518, E-21 Santiago, Chile. (mfarias@dgf.uchile.cl)

B. Poisson, Hazard Mechanisms and Simulation Unit, BRGM, 3 avenue Claude-Guillemin, BP 36009, F-45060 Orléans CEDEX 2, France.

R. Vassallo, LGCA, Université de Savoie, Campus scientifique, F-73376 Le Bourget du Lac CEDEX, France. (riccardo.vassallo@univ-savoie.fr)